Impedance Spectroscopy to Measure Placental Barrier Integrity

by

Karim Saadé

A thesis
submitted to the University of Ottawa
in partial fulfillment of the
thesis requirement for the degree of
Master of Applied Science
in
Mechanical Engineering

Declaration of Authorship

I hereby certify that this thesis is entirely my own original work except where otherwise indicated. I am aware of the University's regulations concerning plagiarism, including those concerning consequent disciplinary actions. Any use of the works of any other author, in any form, is properly acknowledged at their point of use.

Abstract

Various placenta models have been developed, including in-vivo, ex-vivo, and in-vitro approaches, aiming to provide a better understanding of the placental barrier and its interactions with medicinal drugs during pregnancy. The in-vitro model and specifically the placenta-on-a-chip models have shown significant promises as an alternative to conventional in-vitro, in-vivo, and ex-vivo models for investigating the fetal exposure to drugs administered to pregnant mothers. The use of non-invasive techniques allows for continuous monitoring of barrier integrity without damaging the cells. One technique allowing such monitoring is called bioimpedance spectroscopy to measure the transepithelial/transendothelial electrical resistance (TEER) and the electrical capacitance of cell membrane. The aim of this thesis is to *(i)* Design and optimize a low cost, effective and reproducible impedance measuring device to assess the placenta barrier permeability changes; *(ii)* Measure and track electrical properties of a monolayer of epithelial cells to validate the setup; *(iii)* Capture and process syncytialisation data from TEER to correlate with the cell fusion index obtained from immunofluorescence imaging and *(iv)* Propose a Lab-on-a-Chip (LOC) design to mimic a physiological placental barrier in-vitro. We show that the developed impedance spectroscopy system is suitable to measure and track barrier permeability. The measurements confirmed the formation of a confluent monolayer at Day 4. The electrical resistance tripled for treated samples showing the formation of a confluent layer. This resistance remained constant for treated samples reflecting the intact cell barrier and retention of the barrier's integrity over the next 3 days. The resistance of the untreated samples remained in an increasing linear trend due to its lack of fusion and multiple layer formation. The measurements show that, at Day 4, the electrical capacitance of the cells decreases for treated sample as opposed to untreated samples. This reflects that the surface area of the BeWo b30 cells decreases when the samples were treated with forskolin.

Acknowledgements

I want to thank Dr. Marianne Fenech and Dr. Fabio Variola for their support, mentorship and patience throughout my studies. The optimism, encouragement and knowledge that you provided allowed me to perform to my best. I would also like to thank Dr. Benoit Charlot, collaborator in Montpellier, France, and his team for helping us design and fabricate the microfluidic chip. I would also like to thank my lab members for their ongoing support in the laboratory, help and knowledge they provided me with.

Table of Contents

List of Tables

List of Figures

Chapter 1

Introduction

This chapter of the report lays out the overall motivation of this research study as well as the goals and objectives of this thesis.

1.1 Motivation

During the course of pregnancy, the placenta facilitates the exchange of endogenous and exogenous substances, including nutrients and oxygen, between the maternal and fetal systems [2] [3]. This temporary yet crucial organ plays a fundamental role in the development and maintenance of pregnancy [2]. Composed of multilayered membranes, the placenta consists of syncytiotrophoblast (STP) and endothelial cells from the mother and fetus, respectively, separated by a thin interstitium [2]. The resulting placenta barrier is a permeable and specialized structure that regulates the transport of nutrients from the mother to the fetus, effectively separating the maternal intervillous space and fetal circulation [2]. Understanding the physiological changes that occur in the placenta during pregnancy and replicating this physiological model are crucial for maintaining a healthy pregnancy. How-

ever, the integrity of the placental barrier is significantly influenced by the placenta model utilized [4].

Previous investigations have primarily relied on postpartum human placentas for experimentation. However, these studies are limited in terms of knowledge gained due to the placenta's short lifespan after delivery, and they only provide insight into the final stages of pregnancy [5]. Additionally, studies conducted on animal models such as sheep and mice have been prevalent over the years for purposes such as toxicity and drug testing. Nevertheless, despite the similarities between animal placentas and human placentas, significant differences exist that hinder researchers from confidently extrapolating these findings to the human placenta, such as variations in spiral arteries and implantation depth. These anatomical and physiological distinctions restrict the generalizability of these findings to humans due to their species-specific nature [6].

Recent advancements in organs-on-a-chip (OOC) technology have showcased its potential for addressing specific health challenges and developing real-world biomedical devices. Investigating placenta development throughout pregnancy yields critical insights into placental transport between the mother and fetus. Therefore, evaluating barrier permeability to specific drugs and assessing drug toxicity is essential for understanding the functionality of both endothelial and epithelial cells [2] [3]. Consequently, numerous placenta-on-a-chip models have been explored over the years to simulate the placental barrier..

In this study, we propose the design and optimization of a cost-effective, efficient, and reproducible measuring device to assess changes in epithelial barrier permeability. The experimental techniques outlined in this thesis will validate the setup and provide a proof of concept for the development of a placenta-on-a-chip utilizing a cell monolayer derived from human trophoblasts to mimic the STP. Additionally, the integration of electrical measurements will enable real-time tracking of permeability changes in the cell layer.

1.2 Objectives

The primary objectives of this study are to:

1. Design and optimize a low cost, effective and reproducible impedance measuring device to assess the placenta barrier permeability changes.

2. Measure and track electrical properties (resistivity and capacitivity) of a monolayer of epithelial cells (BeWo) to validate the setup.

3. Capture and process syncytialisation data from Bio-Impedance Spectroscopy (BIS) to correlate with the cell fusion index obtained from immunofluorescence imaging.

4. Propose and fabricate a Lab-on-a-Chip (LOC) design to mimic a physiological placental barrier in vitro.

These objectives will be accomplished by first determining the best electrode material and configuration for in-vitro measurements while preventing any disturbance of the epithelial monolayer at the surface of the transwell membrane. Second, the electrical impedance of the confluent cell monolayer at different time points will be correlated to the cell fusion index obtained through staining and analysis of cell images using immunofluorescence imaging. Thereafter, induced syncytialisation using forskolin, allowing the cells to fuse at a higher rate, will be performed to validate the setup. The final step will be a preliminary design of a Lab-on-a-chip model, fabricated at Institute of Electronics and Systems at Montpellier, with integrated electrodes to mimic a physiological placental barrier in vitro.

1.3 Background

1.3.1 Placenta Anatomy

The placenta undergoes rapid development during the initial weeks of gestation, and it serves as a temporary yet vital organ throughout pregnancy. Structurally, it is a multilayered membranous entity comprised of syncytiotrophoblast and endothelial cells from the mother and fetus, respectively, with a thin interstitium separating these cell populations [2]. These two layers form the foundation and essential components for the subsequent development of the placental barrier [7]. The fully developed human placenta is characterized by the presence of three primary types of epithelial trophoblasts as seen in Figure 1.1: cytotrophoblasts (CTBs), syncytiotrophoblast (STB), and extravillous trophoblasts (EVTs). CTBs create a singular lining within the stromal cell core, functioning as the origin for replenishing both the STB and EVTs [8].

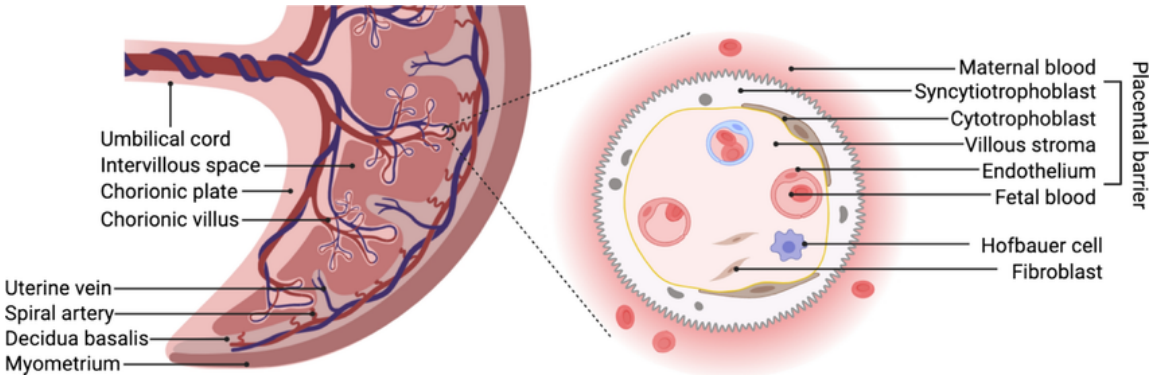

Figure 1.1: Placenta barrier physiology

The different layers making up the placenta barrier are: (1) Synciotrophoblast, multi-nucleated structure differentiated from cytotrophoblasts; (2) Cytotrophoblast; (3) Villous stroma containing the fibroblasts and placental macrophages and (4) Endothelium cells, the fetus cells [8].

1.3.2 Placenta Barrier Function

The placenta assumes a critical role throughout the course of pregnancy, providing vital support for the growth and development of the fetus. It facilitates the exchange of essential substances, including nutrients, oxygen, and waste products, thereby ensuring the well-being and survival of the developing fetus.

An essential function of the placenta is to enable nourishment for the growing fetus. Through the maternal circulation, the chorionic villi extend into the intervillous space (Figure 1.2) and allow nutrients like amino acids, vitamins, and glucose to diffuse across the placental barrier into the fetal circulation and reach the fetus through the umbilical cord. Simultaneously, the placental barrier acts as a filtration system, preventing the passage of harmful substances to safeguard the developing fetus [9].

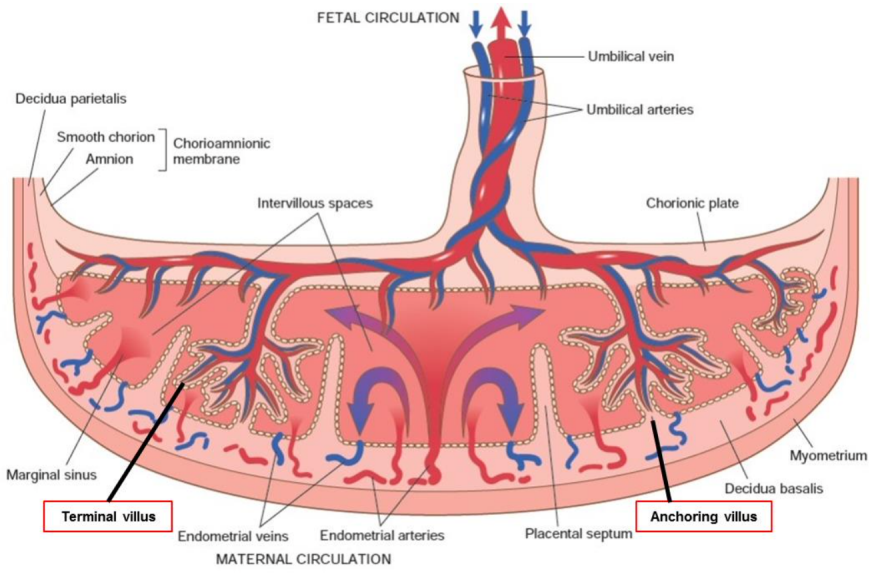

Figure 1.2: Placenta Structure

Adapted from [10].

Moreover, placental exchange is not limited to the unidirectional flow from mother to fetus; it also allows for the elimination of waste products from the fetal bloodstream back to the mother. The placenta transports waste substances, such as carbon dioxide and urea, away from the fetus into the maternal bloodstream, subsequently eliminated through the respiratory and excretory systems [11].

Furthermore, the placenta serves as an endocrine organ and contributes to the maintenance of a healthy pregnancy, particularly in the early stages. It produces a hormone known as human chorionic gonadotropin (hCG) and synthesizes progesterone and estrogen. These hormones play crucial roles in regulating the uterine lining, as well as promoting fetal growth and development [12].

Additionally, the placenta acts as a physical and immunological protective barrier for the fetus. Its selective filtration property prevents harmful substances and pathogens from reaching the fetus. Furthermore, the placenta plays a vital role in immune tolerance by inhibiting the mother's immune cells from attacking the developing fetus. This immune tolerance ensures the fetus can develop without being rejected by the maternal immune system [13].

1.4 Placenta Models

In certain situations, the use of medicinal drugs during pregnancy becomes necessary, particularly in patients with conditions such as diabetes, epilepsy, or bipolar disorders. However, the risks of fetal development from most of these drugs remain uncertain, and there are limited models available to accurately predict the transportation of xenobiotics across the human placental barrier. To address this limitation, various placenta models have been developed, including in-vivo, ex-vivo, and in-vitro approaches. These models

aim to provide a better understanding of the placental barrier and its interactions with medicinal drugs during pregnancy [14].

1.4.1 Conventional Placenta Models

Historically, extensive research on the placenta has been conducted using animal models in-vivo models. Large animals like sheep have been particularly valuable due to their similarities to the human placenta in terms of size and gestational period. However, the accessibility of these animal models has progressively declined, thereby limiting their utility [6]. Numerous studies have explored sheep and mice as models for toxicity and drug testing purposes, including investigations on the impact of substances like lithium, homocysteine, and alcohol on mouse placenta, as well as evaluations of triclosan in sheep placenta and functional analyses of both models [5]. Despite the similarities between sheep, mice, and the human placenta, there exist significant differences that impede researchers from confidently extrapolating these findings to the human placenta. Examples of these disparities include variations in the number of spiral arteries and shallow implantation. These discrepancies in placental anatomy and physiology impose limitations on the applicability of research findings to humans, as these limitations are species-specific [6].

The second, ex-vivo model, was conducted by Panigel et al. in 1967. Subsequently, Schneider and Miller made further advancements in this technique. Both research groups focused on investigating placental pathologies while minimising any potential risks to the mother and the fetus [15]. The extracted placenta, obtained after the delivery of the neonate, is carefully placed in a controlled temperature environment. Artery-vein catheterization and establishment of circulation within the intervillous space are performed. This ex-vivo approach has proven valuable in previous studies, enabling researchers to gain insights into transplacental transfer kinetics and immune responses, including drug transport,

environmental pollutants, addictive substances, infection, and inflammation [15]. However, certain limitations persist in this methodology. Firstly, there are challenges associated with setting up the placenta and meeting its physical requirements. For instance, obtaining a placenta from cesarean delivery is preferable over vaginal delivery. Additionally, the placenta must be physically intact, without any macroscopic tears. Secondly, the lifespan of the placenta following birth is relatively short, allowing for perfusion for a maximum of 48 hours. In addition, inter-individual variations exist when studying transplacental transfer kinetics and immune responses in the placenta. Finally, this method provides insights on the mature and developed placenta at the final stage of pregnancy [15].

1.4.2 Placenta-on-a-chip Models

Placenta-on-a-chip systems have shown significant promise as an alternative to conventional in vitro, in vivo, and ex vivo models for investigating the fetal exposure to drugs administered to pregnant mothers. These systems are not only well-suited for studying transport across the placental barrier in healthy conditions but can also be expanded to include cell lines from placental tissue obtained from women with preeclampsia, facilitating the investigation of placental transport under pathological conditions [14].

Two types of microdevices are employed to mimic the placenta. The first type consisted of multilayered structures with distinct maternal and fetal channels, separated by a thin semipermeable membrane. The second type involves a chip design featuring parallel lanes, each separated by an extracellular matrix (ECM), to represent both the maternal and fetal sides of the placenta. Chips can be fabricated in-house using soft lithography techniques, employing polydimethylsiloxane (PDMS) as the material or commercially available microdevices can be utilized [14].

The dynamic environment of the placenta is simulated by connecting a perfusion system

to the microchannels. This approach is crucial to replicate the physiological and functional conditions of the placenta in vivo. Hence, key factors such as the pore size of the porous membrane, the choice of ECM, the flow rate, and the generated shear stress play a vital role in replicating the human placental environment accurately [14].

In Figure 1.3 and Figure 1.4, various placenta-on-a-chip designs utilized in academic settings can be observed, focusing on studying nutrient transport such as glucose, drug cytotoxicity and placental response on nanoparticles.

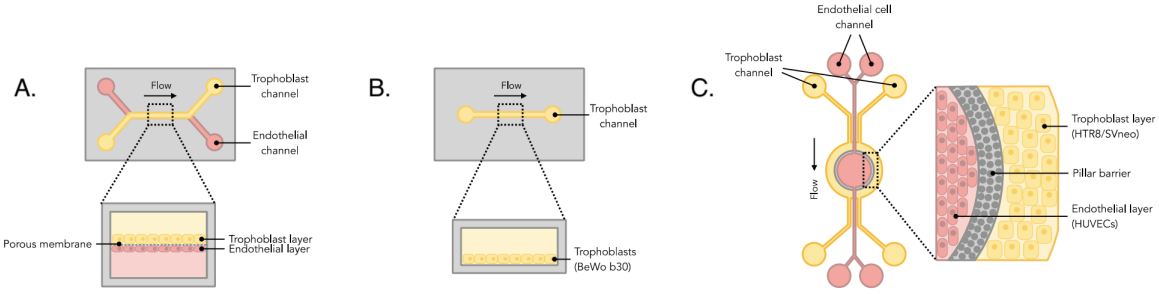

Figure 1.3: Different placenta-on-a-chip models with semipermeable membrane

(A) *Placental barrier chips with two channels configuration, wherein placental trophoblasts (such as BeWo b30) are cultured in one channel and endothelial cells (HUVECs) in the other, both separated by a porous membrane [2].* ***(B)*** *The commercially available microchip iBidi μ-Slide $I^{0.4}$ [14].* ***(C)*** *The SynVivo 3D microchip, a layer of PDMS pillars separate the trophoblasts and endothelial cells allowing cell migration and molecule movement across the two layers [16].*

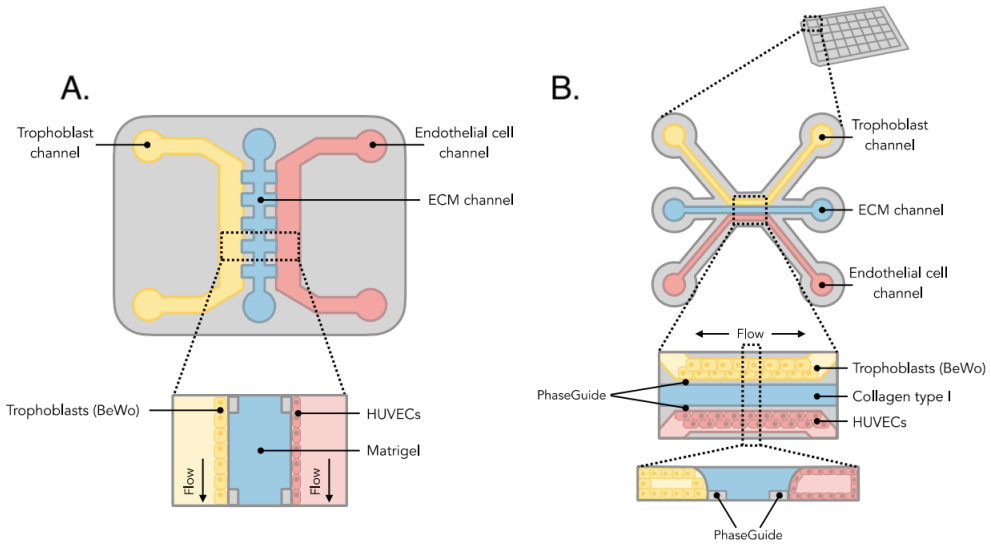

Figure 1.4: Different placenta-on-a-chip models with ECM

(A) *The microdevice utilized in this study is based on polydimethylsiloxane (PDMS) and consists of three parallel channels. The two outer channels are designated for the cultivation of cells, namely trophoblasts represented by BeWo and endothelial cells represented by HUVECs. The central channel, on the other hand, is specifically designated for the extracellular matrix (ECM) component, where Matrigel is employed [17].* ***(B)*** *3-lane Organoplate configuration, where the channels are seeded with trophoblasts (BeWo in this context), ECM (Collagen type I, or a combination of Collagen type I and IV), and endothelial cells (HUVECs) [18].*

Essentially, placenta-on-a-chip systems are microfluidic devices that combine both maternal and fetal channels, separated either by a coated porous membrane coated or by a gel layer of ECM. Notably, the creation of a dynamic environment within an in-vitro placenta is of utmost significance, as it seeks to closely mimic the in-vivo conditions of the human placenta, with the properties of the placental barrier playing a pivotal role in achieving this objective [14].

1.4.3 In-vitro Cell Cultures

Given the disparities between animal and human models, as well as the challenges associated with obtaining and maintaining human placental samples, in-vitro models have been developed to overcome these obstacles.

As an initial approach, primary human cytotrophoblast cells spontaneously differentiate into syncytiotrophoblasts. However, they do not form a polarized confluent monolayer, thereby impeding the study of transcellular transport processes [19]. Rothbauer et al. compared four different human trophoblast-derived cell lines to determine the most suitable model for studying transplacental transport and modeling the placenta. They found that the BeWo cell line, in comparison to the other three cell lines, exhibited the most favorable characteristics for syncytial fusion studies. The remaining three cell lines did not form syncytia, which is a critical parameter in placental development at approximately three months [4]. Hence, BeWo cells became the norm to study transplacental transport and modelling the placenta. BeWo cells derived from a human choriocarcinoma, a malignant tumor characterized by excessive production of the pregnancy hormone, were initially isolated by Roland A. Pattillo. This tumor comprises proliferating cytotrophoblasts with varying degrees of syncytial differentiation [20].

The derivation of the BeWo cell line and the isolation of a specific clone, BeWo b30, from the parent cell have enabled the demonstration of various placental trophoblast properties, including barrier capacity, hormone release, and expression of glucose transporters. This particular BeWo clone has proven to be a vital model for in-vitro human cell culture studies. This BeWo clone is particularly advantageous for such investigations due to its stability, ability to rapidly form a polarized confluent monolayer, and its ease of use and maintenance through subculturing. Additionally, cyclic adenosine monophosphate (cAMP) or forskolin treatment is necessary to induce differentiation and allow the cells to

exhibit morphological characteristics resembling the fusion of cytotrophoblasts into syncytia in primary culture, as depicted in Figure 1.5 [19]. Trophoblast fusion is facilitated by the activation of the glial cells missing 1 (GCM1) transcription factor. The classical fusion peptide syncytin-1, a target gene of GCM1, directly participates in cell fusion. Forskolin triggers an elevation of intracellular cAMP levels by activating adenylyl cyclase. This increased cAMP level subsequently leads to the expression of the GCM1 protein through the activation of protein kinase A (PKA) [21]. Liu et al. conducted a study to investigate the effect of different concentrations of forskolin in the media, ranging from 0 to 35 µM, in order to determine the optimal concentration with low cytotoxicity and efficient syncytial fusion of BeWo cells. They concluded that a concentration of 20 µM was optimal for achieving a balance between effective fusion and minimal cytotoxicity [22]. Moreover, Liu et al. demonstrated the suitability of the BeWo cell line, with forskolin treatment, as a valuable model for in vitro studies on metabolism and transplacental transport. Morphologically, the BeWo cell line exhibited consistent and similar features to syncytialized primary cultures. They showed that with forskolin or 8-BrcAMP treatment, the cell line effectively regulated transport systems in addition to inducing morphological changes [19]. However, the use of forskolin for cell differentiation poses challenges to other cellular properties. Al-Nasiry et al. demonstrated that forskolin treatment led to reduced proliferation rate and cell viability in BeWo cells. Their findings revealed a significant decrease in cell proliferation, with rates decreasing from 4% in control cells to less than 0.7% in forskolin-treated cells [23].

However, the use of BeWo cells alone does not completely model the placenta. As mentioned previously, the placenta is a multi-layer structure composed of both the fetus and the mother cells, separated by a thin interstitium. Therefore, to more precisely mimic and model the placenta, the presence of fetal blood flow and vascularity are necessary in

co-culture with BeWo b30. Human Umbilical Vein Endothelial Cells (HUVECs), derived from the endothelium of the umbilical vein, are mainly used to model the vasculature or blood vessels within organs [24]. These cells, when a monolayer is formed, mimick the inner lining of blood vessels; therefore their use in in-vitro cell culture is essential to model the vascular structure of the placenta [25]. Moreover, the interaction between HUVECs and BeWo cells is significant in understanding the placental-vascular interface. In fact, it was found that both cell lines contribute to permeability studies for size-specific molecules. However, the BeWo b30 layer had a more significant impact on the permeability of smaller molecules [26].

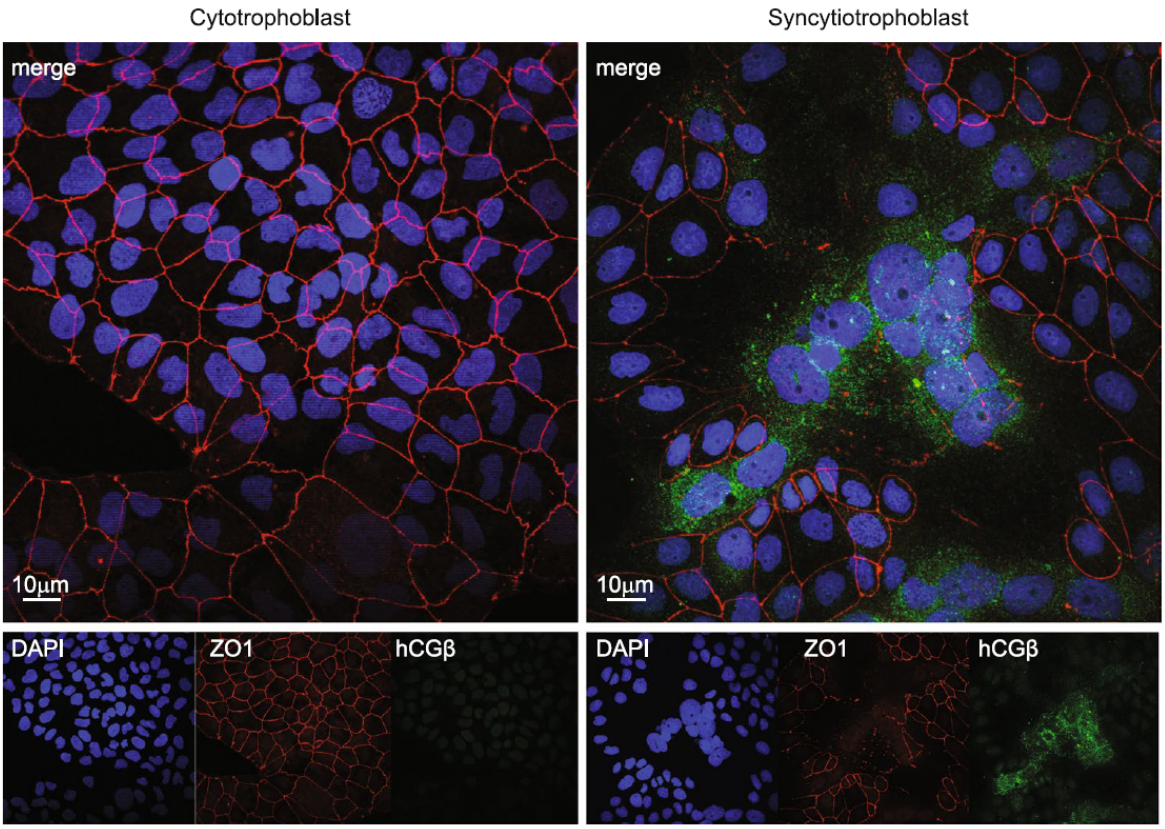

Figure 1.5: Cytotrophoblasts differentiation

(a) Immunofluorescence of BeWo cytotrophoblasts (left) and syncytiotrophoblasts (right). BeWo cells without forskolin (cyt) and with forskolin (syn), were fixed, and nuclei were stained with DAPI (shown in blue), while cell junctions were stained with anti-e-cadherin antibody (shown in red) [2]

1.5 Measurement and Analysis of Barrier Integrity

Given the establishment of the BeWo b30 cell line as a reliable in vitro model for studying metabolism and transplacental transport, it is crucial to evaluate and quantify the barrier permeability to ensure accurate and consistent results. This can be accomplished through techniques such as immunofluorescence staining and impedance spectroscopy.

1.5.1 Cell Fusion Index

As previously explained, the addition of forskolin induces the differentiation of cytotrophoblast cells into syncytiotrophoblasts, leading to their fusion into multi-nucleated structures. The degree of nuclei fusion can be assessed by calculating the fusion index (FUI) using the following relationship.

$$\text{FUI} = \frac{\sum n_f}{N} \tag{1.1}$$

Where n_f is the number of multi-nucleated cells in a field and N is the total number of nuclei of the same field.

Azar et al. observed that treating BeWo b30 cells with a concentration of 100 μM forskolin for 72 hours resulted in an increase in the fusion index from 3.82% to 36.2% [27]. Similarly, Matsukawa et al. found that treatment with 50 μM forskolin led to an increase in cell fusion from 3% to 15% in BeWo parent cells. These findings indicate that the extent of cell fusion is dependent on the concentration of forskolin employed in the experiments [28].

1.5.2 Transepithelial/Transendothelial Electrical Resistance of Cells

In order to visualize the tight junctions and the syncialisation process of the cells to determine the creation of a tight barrier, the cells need to be fixed, permeabilize and stained.

This process prevents any further studies, such as nutrient transfer, drug toxicity studies. In addition, the use of cell trackers in cell culture during transport study can interfere with the study process and affect barrier integrity. Moreover, their use prevents further experiments and renders the cells being tested unusable. Therefore, the use of non-invasive techniques allows for continuous monitoring of barrier integrity without damaging the cells and barrier [29]. One technique allowing such monitoring is called transepithelial/transendothelial electrical resistance or TEER.

TEER measurements is the measurement of electrical resistance across a cellular monolayer and a technique to noninvasively monitor barrier integrity and syncylization during various stages of cell growth and differentiation [30]. By correlating the electrical properties of the epithelial layer, TEER allows the measurement of thickness, tight junction formation, cell layer confluency and morphology [31].

The quantitative measure of the barrier integrity is obtained by measuring the electrical resistance of a cellular monolayer. Figure 1.6 shows the classical setup for TEER measurements. It consists of a cellular monolayer cultured on a semipermeable filter insert. The chopstick electrodes are placed in the bottom and upper compartment separated by the monolayer. By applying a direct current voltage to the electrodes and measuring the resulting current, the Ohmic resistance can be calculated. Using Ohm's law, the Ohmic resistance can be obtained. However, DC current can damage both the cells and the electrodes [29]. Therefore, using an alternating current in the form of a square wave can prevent the damage at frequency equal to 12.5 Hz. The resistance of the tissue (R_{tissue}) can therefore be obtained by subtracting the total resistance (R_{total}), the resistance across the cell layer on the semipermeable membrane, and the blank resistance (R_{blank}), the resistance of the semipermeable membrane alone, without the cells [29].

$$R_{tissue} = R_{total} - R_{blank} \tag{1.2}$$

In addition, it was shown that there exists an inversely proportional relation between the resistance of the tissue to the effective area of the semipermeable membrane (M_{area}). Therefore, TEER values are reported in Ohms.cm^2 and calculated as follows [29].

$$TEER = R_{tissue} M_{area} \tag{1.3}$$

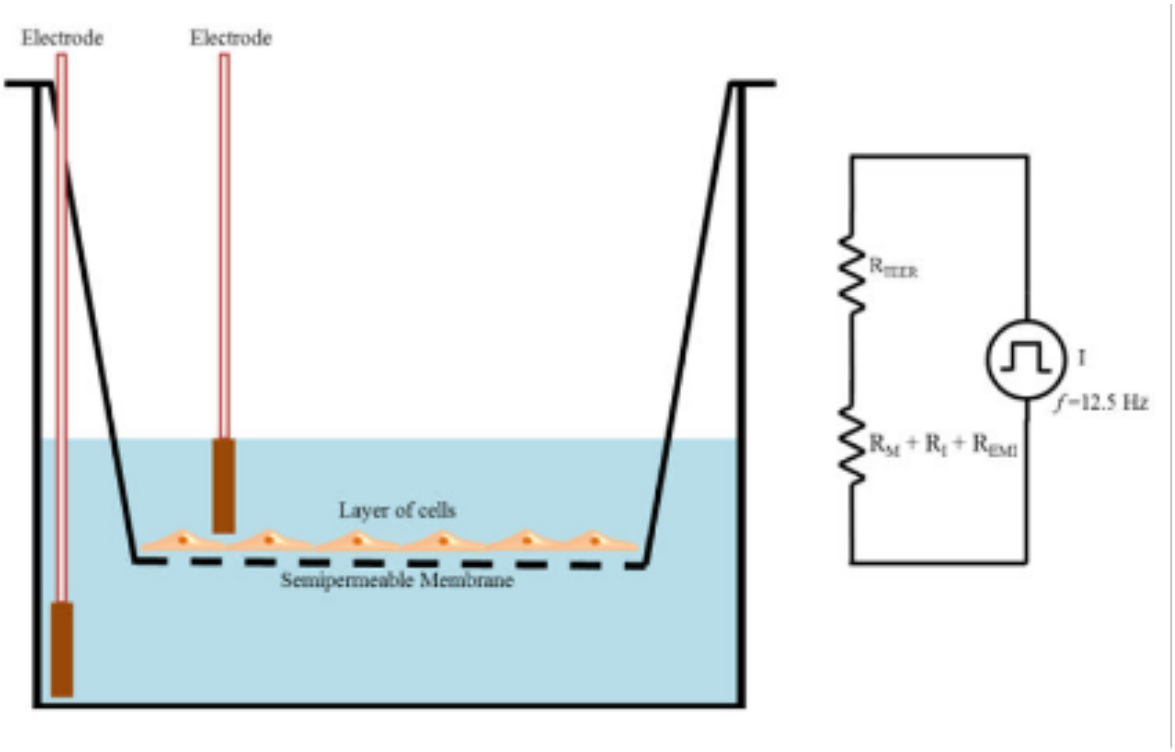

Figure 1.6: TEER measurement with chopstick electrodes

As BeWo b30 cell line is capable of forming a polarized confluent layer, it was shown that they are able to generate a trans-epithelial electrical resistance due to tight cell junction

formation. In fact, Rothbauer et. al. have shown that the TEER increases as a function of days post-seeding of BeWo b30 starting from 100 $\frac{\Omega}{\text{cm}^2}$ to 150 $\frac{\Omega}{\text{cm}^2}$ over a period of 7 days. Moreover, they have shown that TEER is dependent on the cell density. The higher the number of cells the higher the value of TEER [4]. Liu et. al. have also shown the ability of this cell to response to electrical stimulate due to tight junction formation. The TEER increased from about $0\,\Omega\,\text{cm}^2$ to $65\,\Omega\,\text{cm}^2$ from Day 1 to Day 7. The peak resistance was obtained on Day 4, when the cells form a confluent monolayer. TEER then stabilized from Day 4 to Day 7 indicating an intact monolayer. In fact, the addition of 10 mM of EDTA showed a substantial decrease in TEER indicating a change in the barrier permeability [19]. Finally, Tang et. al. confirmed the formation of a confluent monolayer using TEER. At Day 05, TEER reached peak value of about 70 $\frac{\Omega}{\text{cm}^2}$ where it stabilized thereafter due to the intact BeWo b30 barrier [32].

These findings show that BeWo b30 are able to form a tight junction where electrical resistance can be measured to assess the barrier integrity of these cells. By applying an AC in the form of a square wave, barrier integrity assessment can be achieved for the purpose of understanding the effect of certain drugs or medication on the placenta. There exists variations in terms of the value of the TEER measurements between different studies. This can be due to multiple factors such as temperature, position of the electrodes, media compositions. However, the trend obtained remains the same where there is a sharp increase when cells become confluent followed by a constant trend depicting the intact monolayer of the cells.

However, biological cells do not restrict current only; but, they more generally impede electrical current over a wide frequency range giving rise to Bio-Impedance Spectroscopy (BIS) of cells [33].

1.5.3 Bio-Impedance Spectroscopy of Cells

Biological tissues are able to impede electrical current allowing the measurement of electrical property of the tissue. In fact, BIS provides a more accurate representation of the electrical properties that biological cells exhibit. It not only allows the measurement of TEER but also the electrical capacitance of the cell. The response of electrical excitation, via current or potential, of the biological tissue can be measured using electrodes. By applying an alternating current or AC with a frequency sweep, the electrical impedance (Z) can be calculated as the ratio of the voltage (V) and current (I). The electrical impedance is composed of resistive (R), capacitive (C) and inductive (L) components of the system and biological tissue [34].

$$Z = \frac{V}{I} \tag{1.4}$$

Where Z is the complex impedance function composed of the real and imaginary part as shown in Equation 1.5.

$$Z = a + ib \tag{1.5}$$

Where a is the real part, representing resistance and b the imaginary, representing capacitance.

Two resistive pathways are generated in biological tissues. The physical properties of biological tissues, composed of cells with membranes, surrounded by extracellular fluids, create two electrically conducting compartments: the paracellular (or extracellular) and transcellular (or intracellular) media as shown in Figure 1.7.a. These compartments generate resistive pathways describing the flux of ion through the barrier giving rise to TEER and through the cell nuclei respectively. In addition, the semipermeable membrane of the

cells, an insulating lipid bi-layer, gives rise to a capacitive property describing the phospholipid membrane behaviour. However, it was found that the electrical model can be simplified because of the negligible resistive effect of the cell's nuclei [35] [36] [37]. The complete equivalent circuit can be seen in Figure 1.7 and the simplified model is shown in 1.8 and the simplified mathematical model is shown below:

$$Z = R_{media} + \frac{R_{TEER}}{1 + j\omega R_{TEER} C_{cell}} + Z_e \tag{1.6}$$

Where C_{cell} is the capacitance of the cell, R_{TEER} is the trans-epithelial electrical resistance, R_{media} is the resistance of the media and Z_e is the impedance of the electrode.

When analyzing cell properties over a range of frequency, Schwann et. al. reported three distinct dispersion categories: (1) α-dispersion at low frequency, (2) β-dispersion at radio frequency and (3) γ-dispersion at microwave frequency [38]:

1. α-dispersion (10 Hz to a few kHz): At this frequency range, the cell's membrane act as an insulating material preventing any current to flow through the cells. The current flows through the extracellular or paracellular fluid.

2. β-dispersion (100 kHz to several MHz): The current flows through the extracellular and intracellular fluid caused by the polarization of the membrane of the cells.

3. γ-dispersion ($\geq$ GHz): At very high frequencies, the current does not have enough time to flow resulting in the polarization of the water or media.

To obtain the electrical properties of the cells, the optimized region for impedance signal analysis is within α-dispersion frequencies or 10 Hz - 100 kHz. Given the electrical model, TEER and capacitance of the cell membrane can be extracted from the measured impedance in order to obtain a more accurate electrical properties of the cells. Fernandes

et. al. performed impedance spectroscopy on two types of epithelial cells, Caco-2 cells and 16HBE14o- cells, in microfluidic settings. They show that the electrical capacitance property of the Caco-2 cell layer increases over time; on the other hand, the obtained measurement for the 16HBE14o- cells shows a sudden decrease and remains constant over time [39]. Hence, it can be concluded that the capacitive property of cells is cell dependant. In addition, cell capacitance can be influenced by the cell's morphological changes and characteristic such as microvilli formation or other membrane changes such as cell layer thickness [36].

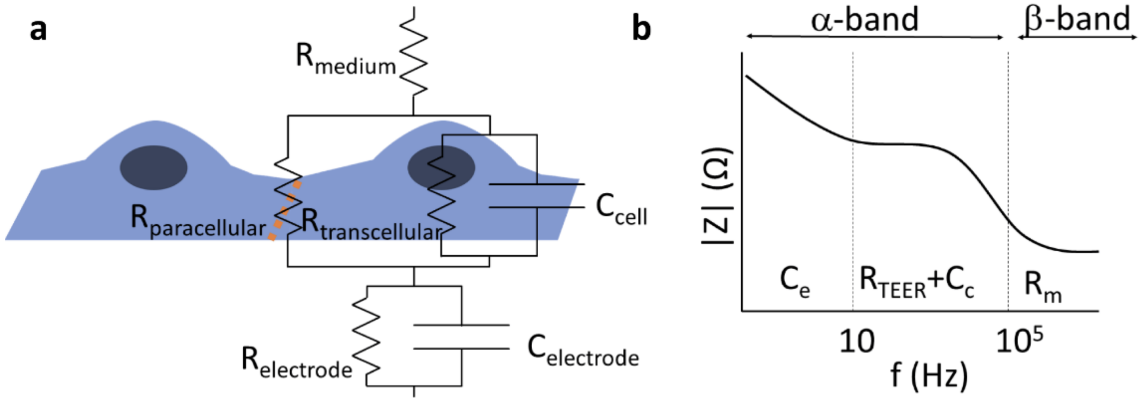

Figure 1.7: Biological cell electrical model

a) Equivalent electrical model for biological cells, C_{cell} *is the capacitance of the cell,* $R_{paracellular}$ *is the extracellular resistance or TEER,* R_{medium} *is the resistance of the media,* $R_{electrode}$ *is the resistance of the electrode and* $C_{electrode}$ *is the capacitance of the electrode.*

b) Graph displaying the theoretical impedance spectra measured and the dispersion categories [37].

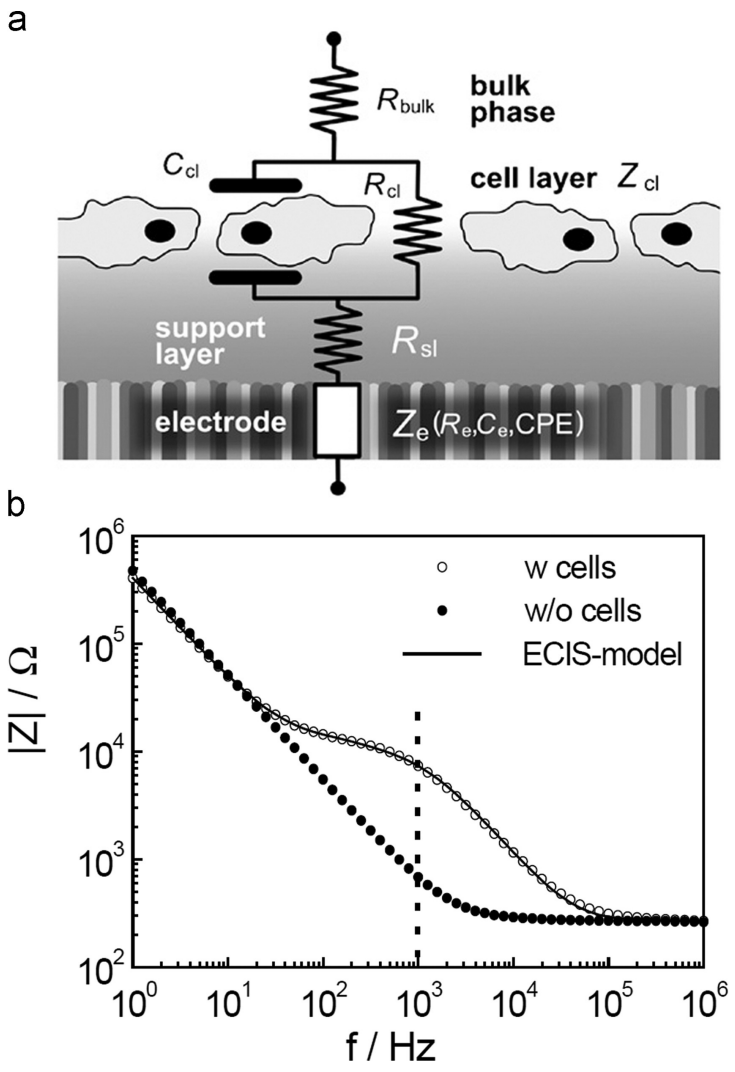

Figure 1.8: Simplified biological cell electrical model

a) Equivalent electrical model for biological cells, C_{cl} *is the capacitance of the cell,* R_{cl} *is the intracellular resistance or TEER,* R_{bulk} *and* R_{sl} *are the resistance of the media and any coating or membrane present and* Z_e *is the impedance of the electrode. b) Graph comparing the theoretical impedance spectra measured with and without cells [35].*

1.5.4 Parameters affecting BIS

Studies have shown that BIS can be affected by multiple factors, such as temperature, cell culture medium composition and shear stress, electrode composition [29], [34].

Temperature have been shown to be a parameter affecting BIS and requires a correction in order to obtain the corrected value. In fact, BIS should be performed in an incubator at 37 °C or at room temperature; however, this requires the samples to reach equilibrium prior to performing the measurements [29]. In fact, Blume et. al. have shown that there is a change in resistance of 2.63 Ω per °K for cell culture inserts without cells and have shown that as temperature increases, TEER values decrease [40]. Hence, it is important to account for this temperature variable.

The second parameter is attributed to media composition. In fact, different laboratories use different protocols and supplementation to grow cells [29]. This in fact changes the media composition and can affect the value of BIS [34]. In fact, it was shown that Caco-2 cells, an epithelial cell line, had lower TEER readouts when different media were used [29].

Given the use of microfluidic device, the presence of shear stress is a core attribute and a parameter that affects BIS values. In fact, non-physiological shear stress can result in restructuring and reorientation of the cells [29]. Cell motility and cell phenotype changes are concurrent with shear stress [41]. These changes can affect barrier integrity and result in TEER changes but also can affect cell membrane and result in capacitance changes . It was shown that under higher shear stress, TEER value increase by 15% from under laminar shear stress [29].

1.6 Conclusion

In conclusion, to this day, traditional methods to monitor placenta barrier integrity, such

as in-vivo, ex-vivo and in-vitro using immunofluorescent imaging, remain heavily utilized. However, each of these methods have their own limitations. Although minor, these limitations can be overcome using simple TEER or BIS. As previously mentioned, BIS allows the measurement of TEER and capacitance property of the membrane lipid bi-layer. These electrical properties allow continuous monitor of the barrier integrity without hindering cell function as opposed to immunofluorescent imaging. From literature, it is evident that there is a correlation between cell density, cell differentiation and TEER that can be observed when BeWo b30 cells are treated with forskolin. As shown in the literature, there is a sharp increase in TEER followed by a constant trend when cells become confluent [2] [19]. In fact, TEER was able to detect permeability degradation of the BeWo b30 monolayer when cells were treated with a 10 mM EDTA solution [19]. On the other hand, the electrical capacitance of the cells is related to the surface area of the cell membrane. Electrical capacitance of cells is very dependent on the type of cells as shown in Fernandes et. al. [39]. We hypothesize that when BeWo b30 cells undergo differentiation, the cell membrane surface area decreases as opposed to undifferentiated cells. Therefore, cell capacitance will decrease. BIS provides the dynamic function of cells as opposed to their structural function. Hence, we propose a low-cost impedance spectroscopy measuring device to monitor BeWo b30 barrier integrity to replace immunofluorescence microscopy. To optimize the readings, several electrode materials will be utilized. Finally, the design and use of a placenta-on-a-chip replicates the physiological and functional conditions of the placenta in vivo by connecting a perfusion system to the microchannels.

Chapter 2

Materials and Methodology

This section of the report will discuss the materials and methodology for culturing, staining and imaging of BeWo cells with the addition of forskolin. In addition, impedance spectroscopy setup and measurements will be detailed in this section.

2.1 BeWo Cell Culture

The subpopulation BeWo b30, derived from the parent cell BeWo and provided by Dr. Alan Schwartz (Washington University in St. Louis), was preserved at -85 °C until ready for thawing. For cell maintenance and growth, DMEM/F-12 cell culture media supplemented with 1% Penicillin-Streptomycin (ThermoFisher), 10% Fetal Bovine Serum (ThermoFisher), and 1% Glutamax (ThermoFisher) was employed [42]. The cell culture media was refreshed every other day to ensure optimal conditions for cell viability and growth.

2.1.1 Thawing Protocol

The cryopreserved cells were retrieved from the -85 °C freezer and thawed in a 37 °C

water bath until the presence of ice was barely visible in the vial. Subsequently, the vial's content was carefully transferred into a 25 mL tube containing 6 mL of culture media. A centrifugation step was then performed to remove any excess solution. The cells were subsequently re-suspended with 2 mL of fresh culture media. For cell culturing, 8 mL of media was dispensed into a T-75 flask, and 2 mL of the cell suspension was added to the flask. The T-75 flask was placed in the incubator at 37 °C with 5% CO_2 to facilitate cell growth and maintenance.

2.1.2 Subculturing BeWo Cells

Cell subculturing was performed when the cells in the flask reached a confluency level of 70-80%. The procedure began with a thorough wash using 10 mL of phosphate-buffered saline (PBS) to remove unwanted debris and dead cells. Subsequently, 5 mL of Trypsin was added to the flask to facilitate cell detachment, and the flask was then incubated for 5 minutes. To inactivate the Trypsin, an equal amount of media was added to the flask. The resulting cell suspension was carefully transferred into a 25 mL conical tube and centrifuged at 400 RCF for 4 minutes. During this step, caution was exercised to avoid disturbing the cell pellet. Subsequently, the supernatant was aspirated, and the cells were re-suspended in 8 mL of culture media. For the next step, 8 mL of media was introduced into a T-75 flask, and 2 mL of the cell suspension was added to the flask. The T-75 flask was then placed in the incubator to support further cell growth.

2.1.3 Seeding BeWo Cells

During the subculturing procedure, BeWo cells were seeded in transwells. In a 1.5 mL microcentrifuge tube, 20 uL of Trypan blue dye was added to differentiate between live and dead cells. Next, 20 uL of the cell suspension was pipetted into the tube and mixed

thoroughly for even cell distribution. Using a hemocytometer, cell counts were performed by placing 10 uL of the mixture on both sides of the hemocytometer and counting cells under a microscope. The average of eight squares was taken, and the total cell count was multiplied by 10,000 to convert it to cells per mL. A correction factor of 2 was applied to account for the 1:1 dilution of cell suspension and Trypan blue. To achieve a seeding density of 100,000 cells/cm^2 on the transwell insert (cellQART - Sterlitech), the total cell count needed was 110,000 cells. To ensure homogeneous distribution, the required cell suspension volume was mixed with the necessary media volume in a 25 mL tube. 500 uL of the mixture was then added to the apical compartment of the transwell insert, and 1.5 mL of media was placed in the basolateral compartment. The cells were washed daily with PBS, and the media was replenished accordingly.

2.1.4 Collagen Coating

BeWo b30 cells have a low attachment rate of about 6% on uncoated substrate as shown by Hohn et. al. [43]. To enhance cell attachment on the un-coated substrate, the membranes of the transwell inserts were coated with Collagen Type IV. Collagen Type IV at 3.4 mg/mL concentration (C_{stock}) was diluted with the addition of DMEM/F-12, 10x PBS and NaOH to obtain a final concentration of 0.1 mg/mL (C_{final}). The volume (V_{final}) required to coat the membrane is equal to 300 μL. The quantity of each of the material should follow the below order:

1. 10x PBS:
$$V_{PBS} = \frac{2V_{stock}}{10} \tag{2.1}$$
2. DMEM/F-12:
$$V_{media} = V_{final} - (V_{stock} + V_{PBS} + 1) \tag{2.2}$$

3. Collagen:

$$V_{stock} = \frac{C_{stock} V_{final}}{C_{final}} \tag{2.3}$$

4. NaOH:

$$V_{NaOH} = 1\,\mu\text{L} \tag{2.4}$$

After coating, the transwell inserts were incubated for 3 hours and excess collagen was aspirated. Subsequently, the inserts were washed with 1x PBS and then ready for use.

To verify the presence of collagen, the inserts were stained with Alexa 555 NHS and observed under fluorescent microscope, AxioObserver Z1 inverted microscope (Zeiss, Germany), at 10x as shown in Figure 2.1.

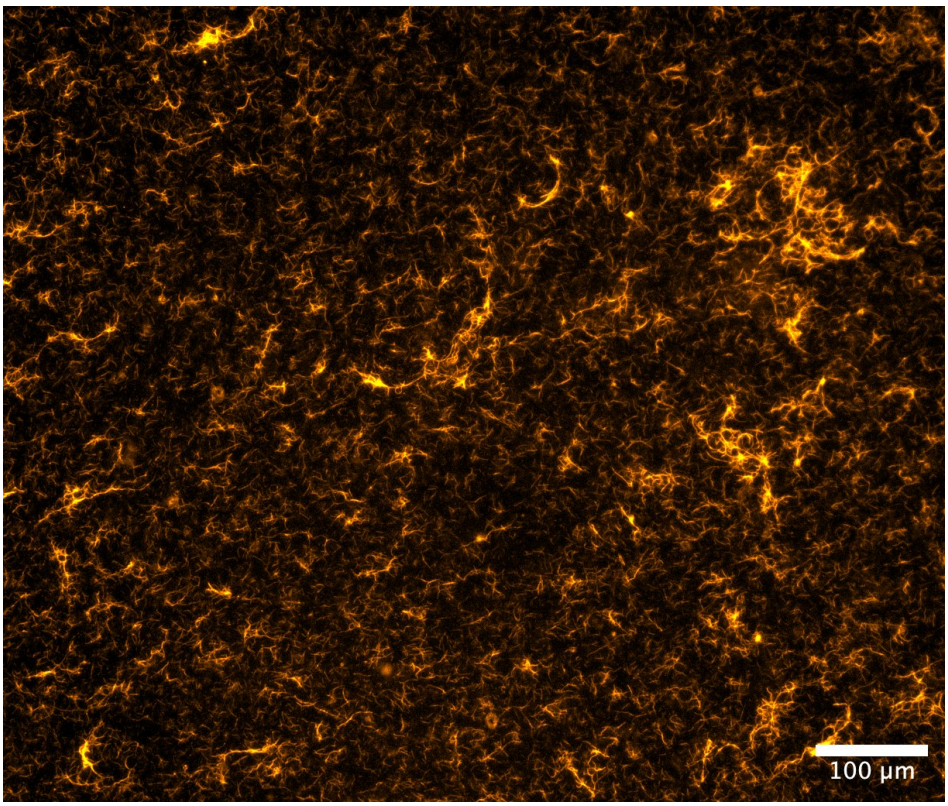

Figure 2.1: Stained Collagen on Polyester Membrane

2.1.5 Differentiation of BeWo b30 cells

To induce differentiation of the cells, a concentration of 20 uM of forskolin was introduced day 2 post-seeding. Stock solution of forskolin at 100 mM was diluted with DMSO at 1:5 ratio to obtain 20 mM aliquots. Finally, the aliquots were introduced in the media at 1 uL of forskolin per 1 mL of media to obtain a final concentration of 20 uM of forskolin.

2.2 Immunofluorescence

2.2.1 Staining

In order to visualize the syncytialisation process of the cells, immunofluorescence (IF) staining was performed. This entails staining for the cells' nuclei and the gap junction. The cells were permeabilized using 4% Paraformaldehyde (PFA) in the transwell for 20 min at room temperature. This will dissolve the cell membrane allowing dye molecules to enter the cell. Following this step, the transwells were washed 3 times with PBS for 2 min and the membranes were cut into four pieces and placed in 24 wells plate. 0.4% Triton-X in PBS was used to fix the cells for 20 min at room temperature. The inserts were then blocked overnight at 4°C in 5% donkey serum and PBS. The next day, the primary antibody, E-cadherin, was diluted at 1:500 with PBS and 5% donkey serum and placed in the wells overnight at 4 °C. Prior to adding the secondary antibody, the cells were washed 3 times for 30 min to remove any unbound antibodies. The secondary antibodies, DAPI (1:1000) and Alexa 647 (1:500), were diluted in PBS and donkey serum and added to the wells for 1 hour at room temperature. Finally the cells were washed 3 times for 30 min. The samples were finally mounted on No. 1.5 glass coverslips using VectaShield, kept to dry overnight at room temperature and store in the fridge the next day until imaging.

Multi-channel images were captured with an AxioObserver Z1 inverted microscope (Zeiss, Germany). Z-stack images were performed for assessment of cell differentiation.

2.2.2 Analysis

Image collections were deconvoluted with ZenPro Software (Zeiss) and focus stacked with ImageJ (NIH). The files were then run through a cell profiler pipeline to quantify the number of nuclei. The remaining cells were then manually counted using QuPath to assess cell fusion index using Equation 1.1. Appendix 4 shows the steps to obtain final count.

2.3 Impedance Spectroscopy

2.3.1 Electrode Setup

In this research, a two-electrode configuration was employed, consisting of a working electrode and a counter electrode. Two electrode materials were used: (1) A 1 mm stainless steel rod coated with conductive paint and (2) the STX-4 electrode purchased from World Precision Instrumentation (Catalogue #EVM-AC-03-01-01). To ensure stability and accurate readings, a 3D-printed support, shown in Appendix 4 was utilized to secure the electrodes and prevent any unintended movement that could potentially interfere with the measurements or cause damage to the cell layer [30]. The first electrode tip was positioned at the centre of the apical chamber, while the second electrode was placed in the basolateral chamber, approximately 7.5 cm away from the first electrode. The height of the electrodes, measured from the support, extended approximately 14 mm into the apical chamber and 17 mm into the basolateral chamber, respectively. The configuration of the electrodes is depicted in Figure 1.6. The experimental setup can be seen in Figure 2.2.

2.3.2 Impedance Reader

Cell impedance measurements were conducted using the Analog Discovery 2 (AD2) device obtained from Digilent. The device generates an AC signal at constant 10 µA with a frequency sweep between 5 Hz - 1 MHz. To minimize the complexities associated with the electrical circuit and mitigate undesired inductance from wiring, a specialized impedance analyzer plug-in specifically designed for the AD2 was purchased from Digilent. Furthermore, this plug-in offered the flexibility of automatically adjusting the reference resistance based on the electrical characteristics of the tested device, thereby optimizing the measurement setup and enhancing accuracy.

2.3.3 Analysis of the Impedance Signal.

For impedance signal analysis, the software ZView was employed. This software enabled the creation of an electrical circuit encompassing the relevant components, including the cells, media, and electrode electrical properties. By fitting the impedance curve from 10 Hz to 100 kHz, ZView facilitated the extraction of resistive and capacitive values, thereby providing valuable insights into the electrical characteristics of the system under investigation. An example of the fit can be seen in Appendix 4.

2.3.4 Statistical Analysis

A paired t-test was performed to determine if there are significant differences among the four different conditions: collagen coated, uncoated substrates, forskolin treated, and untreated samples. The t-test will compare the means of two groups, specifically treated against untreated and coated and uncoated blank inserts, and determine whether there is a statistically significant difference between them.

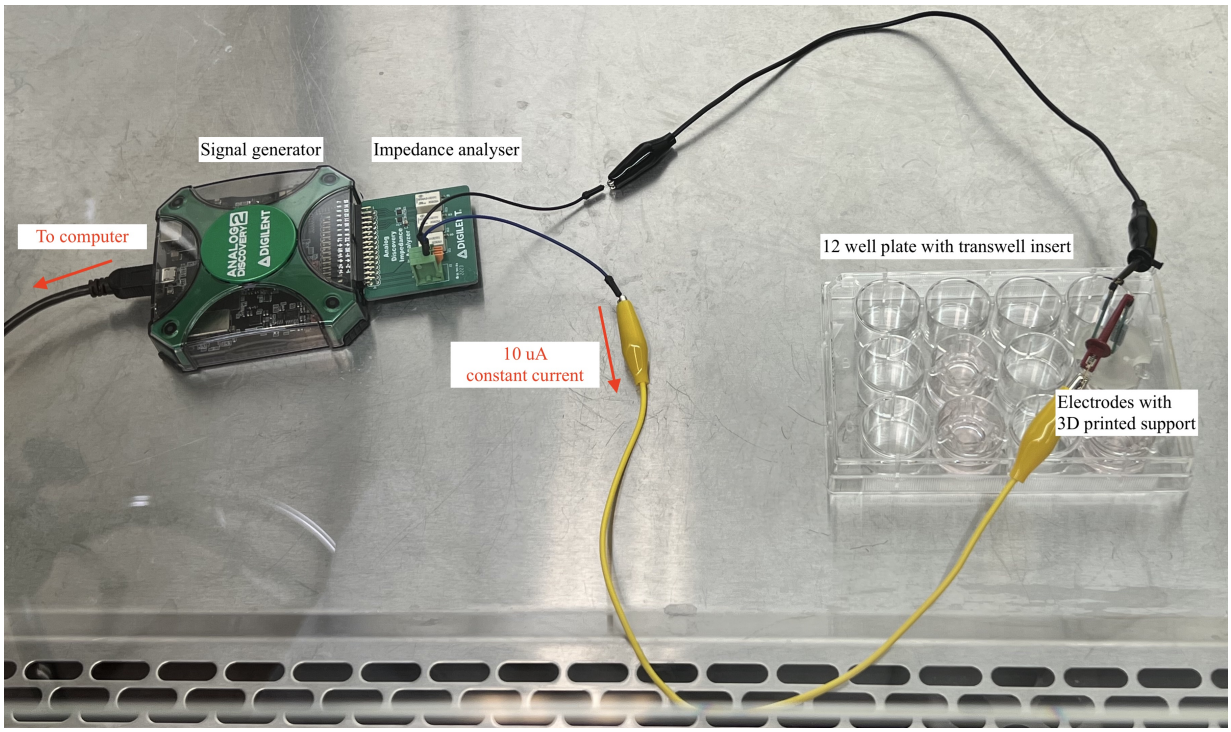

Figure 2.2: Experimental setup

2.4 Microfluidic Device Fabrication

2.4.1 Photolithography

After determining microchannel dimensions (Figure 2.3) and electrode dimensions, a transparency photomask is printed, containing the desired configuration (Figure 2.4), which appears as the black regions of the mask (Figure 2.4A). This geometry is eventually transferred onto a silicon wafer to create the inverse mold.

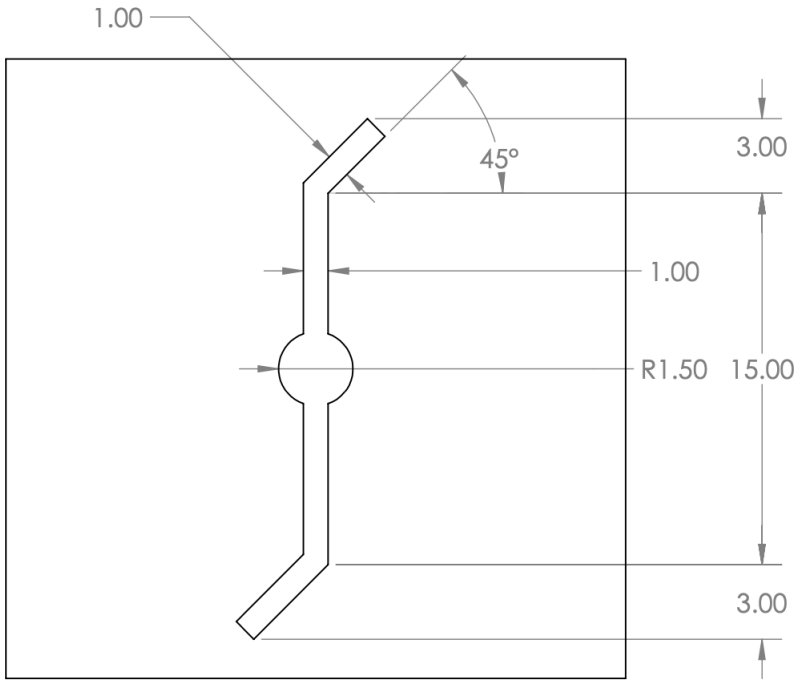

Figure 2.3: Microchannel dimension

Dimensions are in mm. The height of the channel is 100 μm.

The photomask was designed in Solidworks for a 4-inch-diameter silicon wafer. The design was sent to Centre National de la Recherche Scientifique (CNRS) (Montpellier,

France), where it was printed onto a clear cellulose acetate sheet as a high precision photomask.

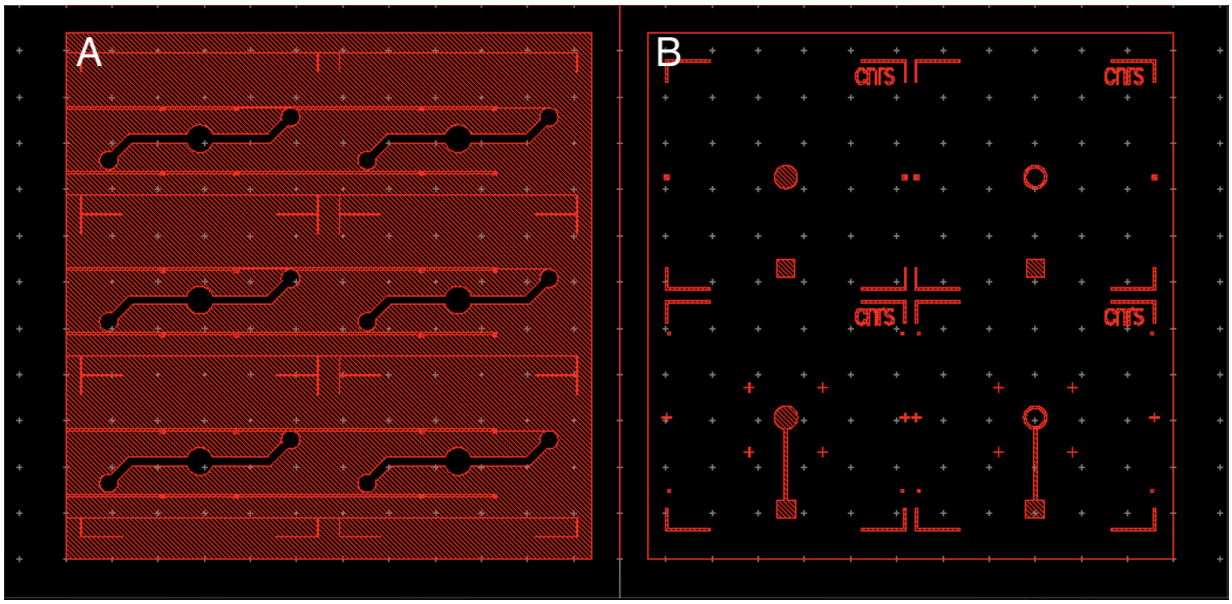

Figure 2.4: Photomask design

A) Microfluidic channel design and B) Electrode design.

The silicon wafer was cleaned in a 1% v/v hydrofluoric acid (HF) solution, allowing for the removal of built up silicon oxide in order to improve surface bonding capability with the photo resist. SU-8 epoxy-based negative photo resist was spincoated on a spread cycle of 500 rpm for 10 seconds, and then 1000 rpm for 30 seconds. This creates the desired thickness of 100 µm, according to the manufacturer's instructions. The silicon, SU-8 coated wafer was soft-baked at 65 °C for 10 minutes, and hard-baked at 95 °C for 30 minutes.

The photo-mask was placed on top of the coated wafer and the assembly was exposed to 350 mJ/cm^2 of UV light for 2 second in a UV box. The transparent regions of the photomask expose the photo resist to the UV light causing it to cure, while the opaque regions block the light. A soft-bake at 65 °C for 3 minutes and then a hard-bake at 95 °C

for 10 minutes was completed to cross-link the exposed regions of the photo resist. After, the assembly was placed in SU-8 developer solution for 10-15 minutes with agitation. This allows uncured regions to dissolve, leaving the elevated cured regions, and forming the inverse master mould for the microfluidic chip (Figure 2.5). The height of the channel was confirmed using a profilometer and was measured to be 97 µm.

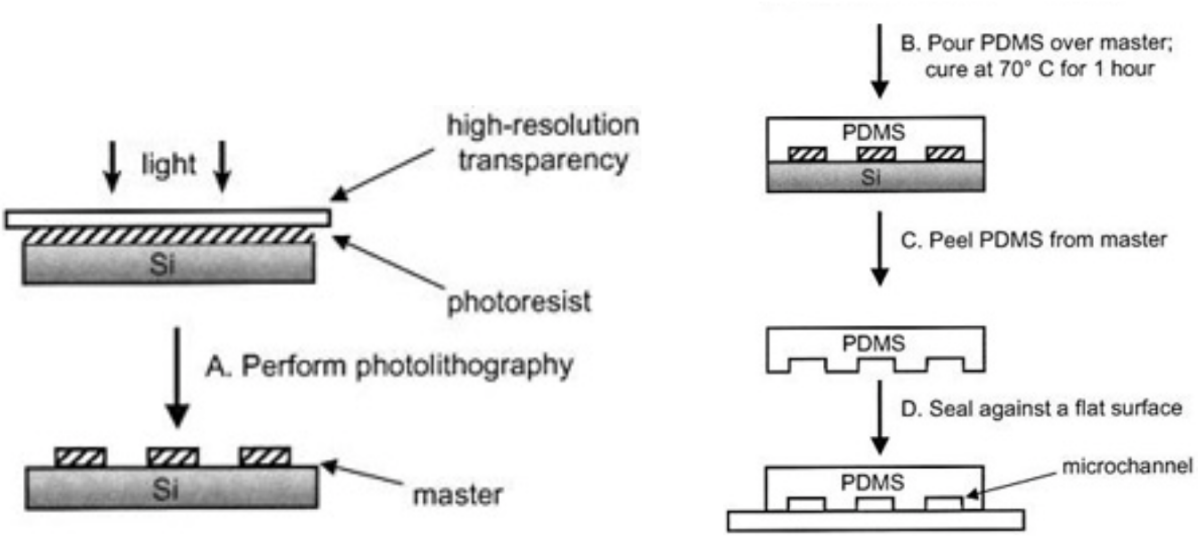

Figure 2.5: Photolithography and soft lithography processes

Adapted from [44].

2.4.2 Soft-lithography method to create channels

A 10:1 ratio mixture of PDMS elastomer base and curing agent, Sylgard 184, was prepared, degassed in a vacuum desiccator, poured on a master mold placed in a Pyrex dish, and cured in the oven for 2 hours at 70 °C. PDMS channels were then peeled from the master mold, cut out, and the middle hole was punched using 3 mm diameter punches.

2.4.3 Electrode Patterning

Prior to resin deposition on glass slide and electrode patterning, the glass slides were cleaned using piranha solution in order to remove any organic residues on the substrate. The glass slides were washed with deionized water and blown dry and exposed to plasma treatment. The glass slide is placed on a preheated hotplate at 110 °C to remove any humidity prior to spin coating. After spin coating a thin layer of negative resin (AZ2020) at 3000 rpm for 30 s on a glass slide, the resin-coated surface was exposed to UV light using the bottom pattern of the mask for the electrode (Figure 2.4 B). The transparent area lets the UV light cure the resin while the blocked light allows the resin to dissolve when exposed to the developer solution. This step will pattern the electrode for the next process, metal deposition. The glass slides were prepared to perform metal deposition by evaporation. A thin layer of titanium, 20 nm was deposited on the glass surface. This layer will essentially act as an adhesive for the 150 nm gold layer. Following the deposition, the glass substrates were placed in the RemoverPG at 80 °C to perform the liftoff and the glass slides were cleaned with IPA and brushed gently. The liftoff process can be seen in Figure 2.6. The electrodes were regularly checked under the microscope to see if gold residue are present (Figure 2.7A). The final electrodes can be seen in Figure 2.7B.

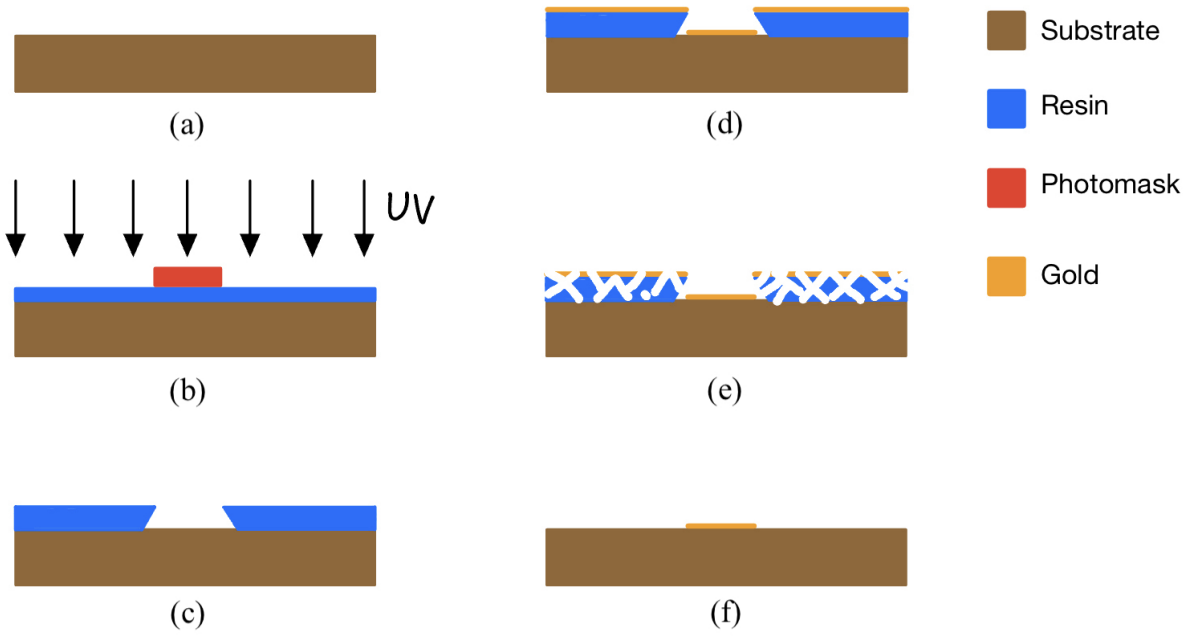

Figure 2.6: Electrodes patterning process

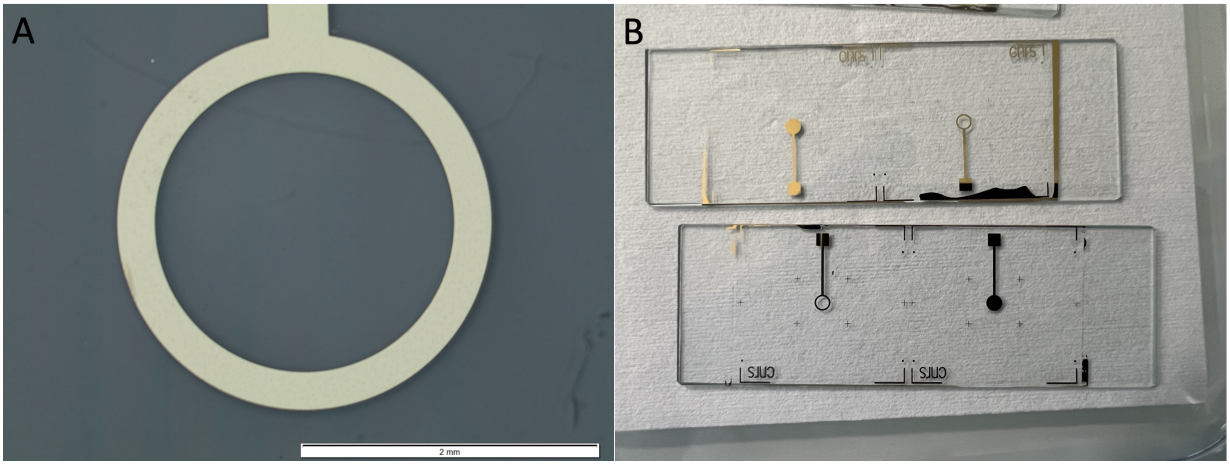

Figure 2.7: Electrode post liftoff

Electrode A) under microscope and B) on glass substrate

An insulating layer of Silicone Nitride, Si_3N_4, was applied to areas where cells are not present or where connections will not be made. The specific area where an insulating layer is not present can be seen on the mask in Figure 2.4B. The insulating layer was deposited for 300 seconds at 280 °C (Figure 2.8(a)). A second lithography was performed (Figure 2.8(b) and Figure 2.8(c)) in order to pattern the area on the glass substrate, following the same protocol as before, and exposed to the plasma for a Reactive Ion Etching (RIE). The Si_3N_4 layer exposed to the plasma was etched for 3.5 min to allow electrode contact with the cells and the wire connection (Figure 2.8(d)). The resin was then etched to clean the substrate and have the Si_3N_4 layer exposed for insulation (Figure 2.8(f)).

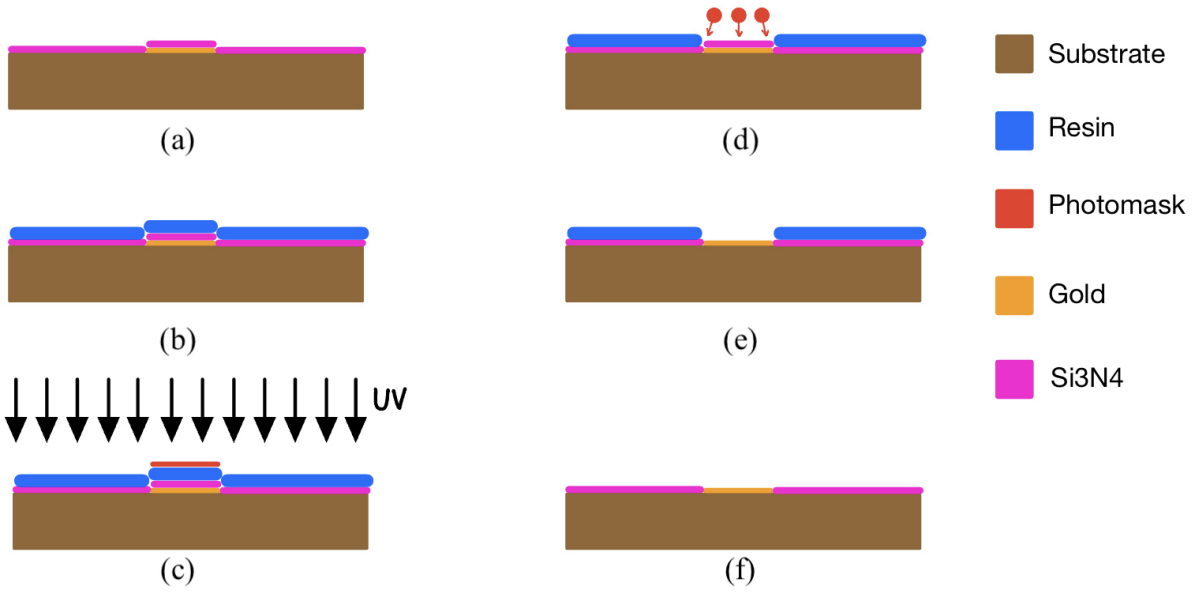

Figure 2.8: RIE process for insulating layer

2.4.4 Chip Assembly

To establish the chip inlet and outlet through the glass slide, the central region of the microfluidic chip, wherein the membrane is to be positioned, was aligned with the electrode ring. Subsequently, a handheld drill equipped with a 3 mm diamond tip was used to perforate the glass. Following this, the glass substrates underwent cleansing procedures using a Piranha solution.

The PDMS material was affixed to the glass substrate through a plasma bonding process. Initially, both the PDMS and glass slides were bonded using plasma treated for 1.5-minute. Subsequent to the alignment, the assembly was positioned on a heating plate set at 90 °C. Membranes were then cut using a 6 mm punch and affixed to the central region of the microfluidic chip.

Finally, the upper and lower channels were bonded. Ultimately, electrical connectivity was established through the application of Silver conductive paint (SCP03B - RS France), allowed to dry overnight. To safeguard the applied coating, NoA 81 optical glue (Norland Optical Adhesive) was used and cured using ultraviolet (UV) for 2 minutes. The finalized configuration of the assembled microfluidic device is depicted in Figure 2.9.

2.4.5 Preliminary Cell Culture Trial

The bonded microfluidic chip with membrane were plasma treated to allow the channel to be hydrophilic in order to sterilize it with ethanol. The chip was then placed under UV light in the biohood for 15 min. The membrane in the chip was coated with Poly D lysine, PDL, for 15 min to enhance collagen coating on the membrane allowing the cells to adhere faster and more effectively on the membrane. Collagen protocol was followed as previously described in Section 2.1.4. HUVECs (CBS, Montpellier) were inserted through

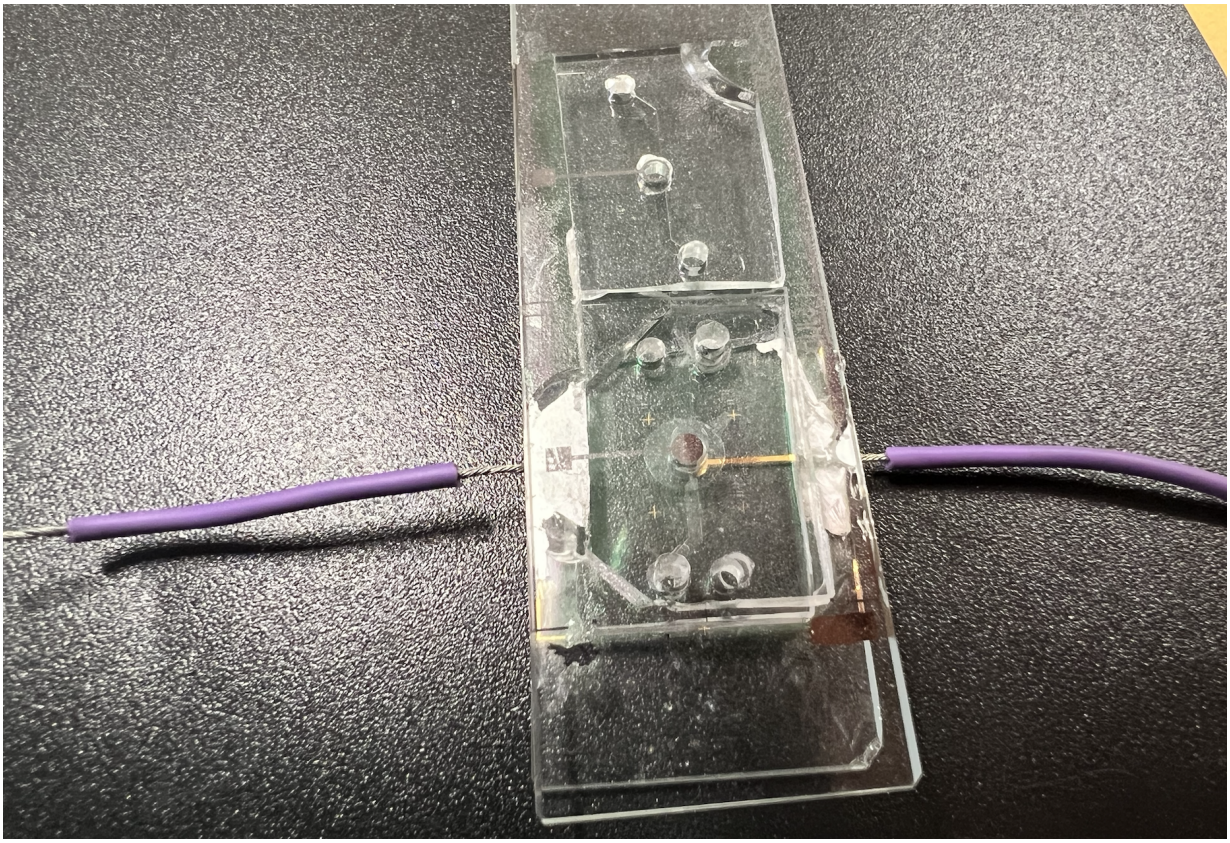

Figure 2.9: Assembled chip

the inlet using a syringe and allowed to settle and attach to the membrane and placed in the incubator for about 4 hours. Subsequently, gravity driven flow was utilised to allow media change overnight. The height difference between the inlet and outlet will allow for flow to occur in order to circulate and replace the media for the cells. The cells were observed under the microscope to assess the growth and attachment of cells.

2.4.6 Preliminary Impedance Measurements

The microfluidic chip was perfused with PBS 1x in order to run impedance measurements

and measure the contribution of the electrode and electrical connection on the system. Similar settings to Section 2.3.2 were used. The setup can be seen in Figure 2.10.

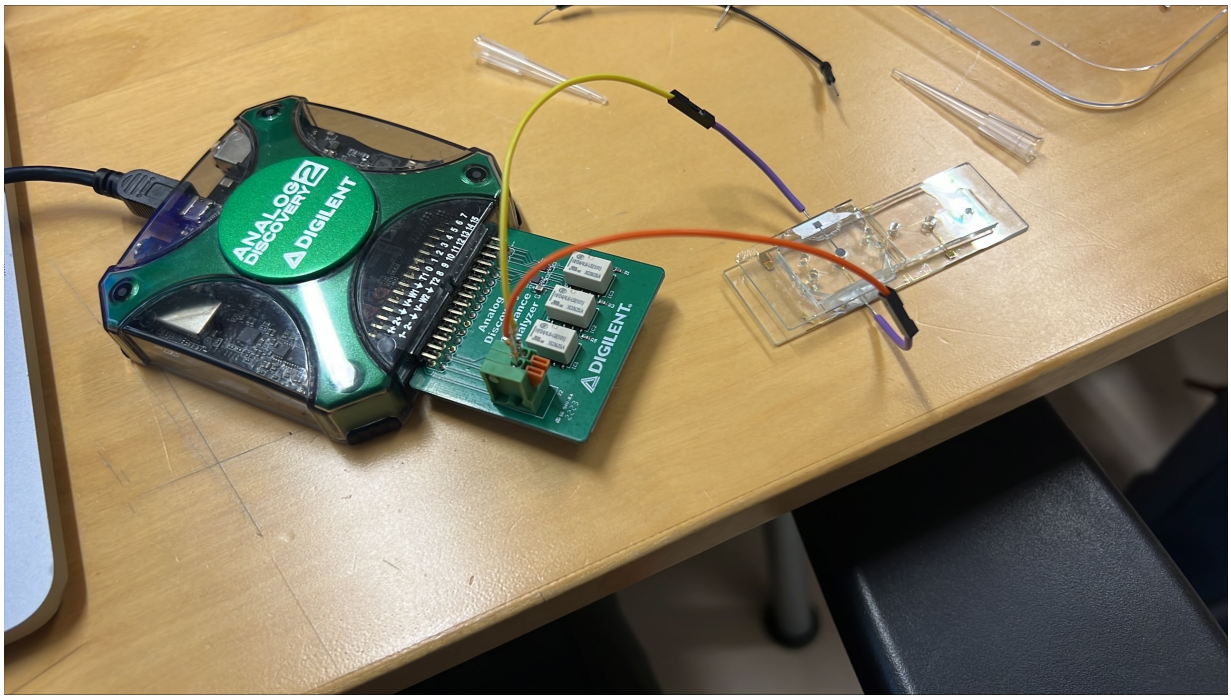

Figure 2.10: Chip with AD2

Nyquist plot was utilised to represent the real and imaginary part onn the cartesian coordinate system. ZView software was used to determine the overall impedance impact of the electrode and wire connection on the system. Given the absence of cells, the electrical model used to fit the curve is shown in Figure 2.11. This model is the typical electrode electrolyte describing a double layer capacitance [45].

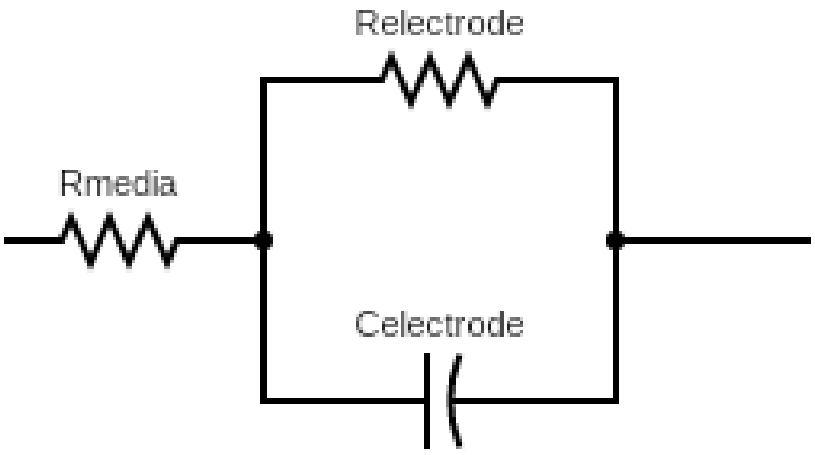

Figure 2.11: Double layer capacitance effect [1]

Chapter 3

Results and Discussion

This section of the report will layout the results of cell fusion index obtained from immunofluorescence imaging and impedance spectroscopy measurements to assess the BeWo b30 monolayer integrity and confirm the viability of the impedance spectroscopy setup.

3.1 Monolayer Formation and Assessment

Figure 3.1 shows the immunofluorescence images acquired at Day 3 and Day 5 post-seeding for samples treated with and without forskolin. As previously mentioned, BeWo b30 cytotrophoblast cells differentiate into syncytiotrophoblast when treated with forskolin. The cells will therefore form a multinucleated structure loosing their cell membrane and allowing cell fusion.

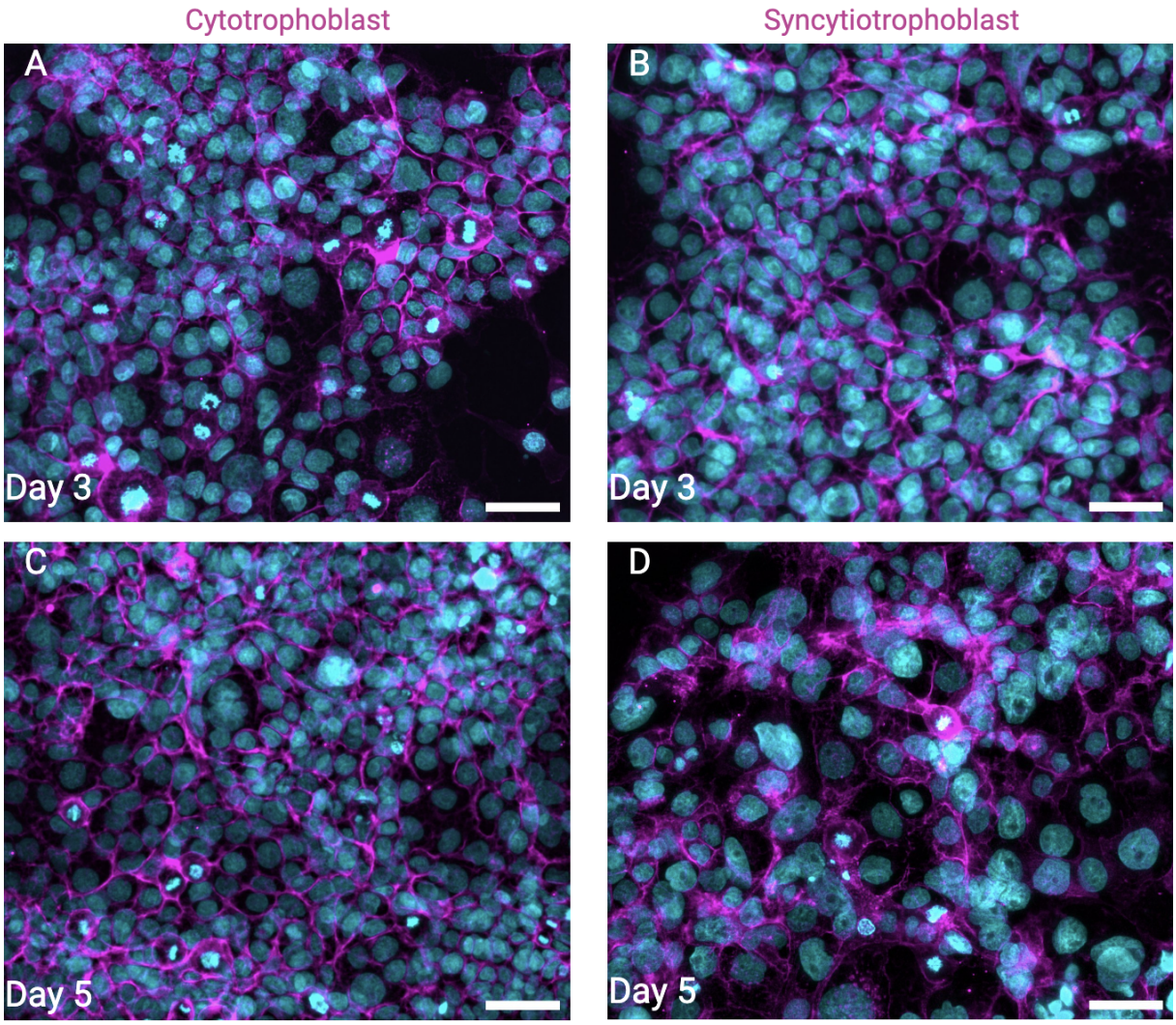

Figure 3.1: Widefield fluorescence microscopy staining of tight junctions of BeWo b30

BeWo b30 cells cultured on the top side of the porous membrane. Magenta shows E-cadherin staining and cyan shows DAPI staining. Scale bar: 55 µm

As can be seen in Figure 3.1A, cells do not form a monolayer as compared to Day 5 (Figure 3.1C). The trophoblast cells show strong expression of E-cadherin illustrating the formation of a confluent and continuous intercellular junctions. When treated with

forskolin (Figure 3.1B and Figure 3.1D), it can be seen that the expression of E-cadherin is weaker, representing a significant loss of intercellular junctions specifically at Day 5. In addition, the cell nuclei observed are bigger suggesting cell fusion as confirmed in Blundell et. al. [2]. A more representative fluorescent image of cell fusion can be seen in Figure 3.2.

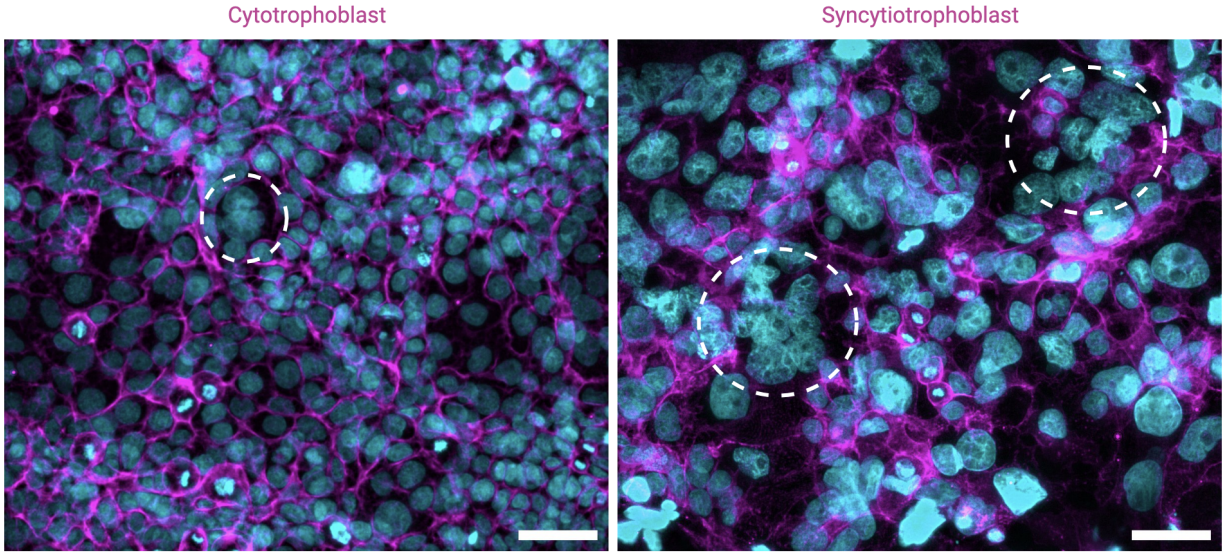

Figure 3.2: Widefield fluorescence microscopy of BeWo b30 Day 4 post-seeding. *Prolonged exposure to forskolin leads to a notable decline in intercellular junctions (depicted in magenta) and prompts syncytialization-like cell fusion (white dashed circle) within a 4-day timeframe in BeWo b30 cells. Scale bar: 55 µm*

To quantify cell fusion, Equation 1.1 will be used with respect to the images acquired from staining. Table 3.1 shows the cell fusion index in percentage for Day 3, Day 4 and Day 5 for control and treated wells. The cell fusion calculated for the untreated wells at Day 3, Day 4 and Day 5 show no increase. On the other hand, there is an increasing trend observed at Day 3, Day 4 and Day 5 for treated wells starting from 7.62% to 17.83%. These results show that in fact cell fusion occurs at a higher rate when cells are treated

with forskolin. The results obtained are lower than the literature review finding; however, the concentration of forskolin utilized in this study is lower. In fact, Azar et. al. have shown that, when BeWo b30 cells are treated with 100 μM of forskolin, the cell fusion index is equal to 36.2% [27]. Moreover, Matsukawa et. al. have shown that the cell fusion index for the parent cells, BeWo, are equal to 15% when cells are treated with 50 μM [28].

As can be seen, none of the above studies reach a 100% fusion rate and it was shown that there is inconsistencies with fusion index between different groups [46]. Wang et. al. have shown that not only the cell type matters but also the staining techniques [46]. In fact, they have shown that there is discrepancies in the fusion index when using 1) primary cytotrophoblasts, which have a higher fusion rate, rather than using BeWo, with a lower fusion rate; and 2) there is difficulty visualising some E-cadherin stained boundary [46]. Moreover, other factors contributing to higher fusion index could be attributed to media composition, concentration of forskolin, method used for the cell isolation and if using a primary cell line, the individual differences derived from donor of cytotrophoblast [46].

Table 3.1: Cell Fusion Index [%]

Days	Control	+20 μM Forksolin
Day 03	3.36±0.91	7.62±2.21
Day 04	3.82±1.10	16.47±1.84
Day 05	3.02±1.21	17.83±2.07

Values are Means ±SD; average n = 9.

A paired T-Test was performed to determine whether there is a statistically significant difference between treated and untreated samples as well as within groups. Table 3.2 shows the p-value obtained for this T-test where F represent treated samples and NF represent

untreated samples. Figure 3.3 shows the statistical data for the cell fusion index. It can be seen that there exists a statistically significant difference between treated and untreated samples at the three different days. In addition, there exists a statistically significant difference within the treated samples groups.

Table 3.2: Paired Samples T-Test for Fusion Index for treated (F) and untreated (NF) samples

Measure 1		Measure 2	t	df	p
F3	-	NF3	5.270	8	$< .01$
F4	-	NF4	20.447	8	$< .01$
F5	-	NF5	21.461	8	$< .01$
F3	-	F4	−9.098	8	$< .01$
F3	-	F5	−11.058	8	$< .01$
F4	-	F5	−2.253	8	0.054
NF3	-	NF4	−0.976	8	0.358
NF3	-	NF5	0.698	8	0.505
NF4	-	NF5	1.634	8	0.141

Note. Student's t-test.

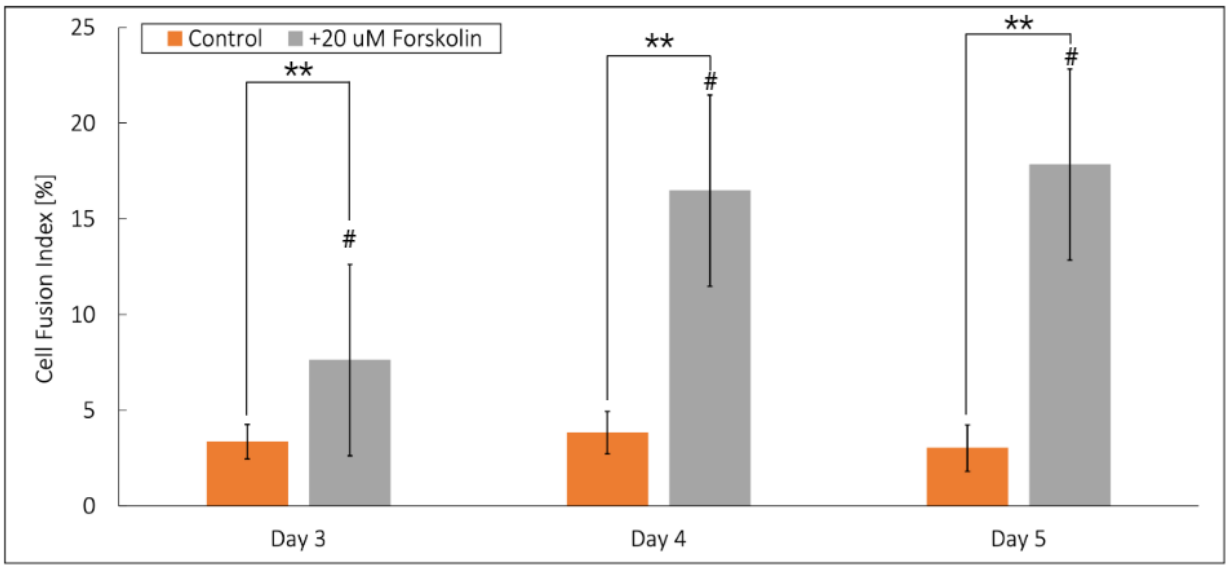

Figure 3.3: Cell fusion index with statistical analysis.

*Monolayer cultures with (grey) and without (orange) forskolin. Data represent Means ±SD from triplicate samples ($n = 9$). * and ** indicate $p < 0.05$ and $p < 0.01$, respectively. # is significantly different from Day 3 ($p < 0.01$).*

In conclusion, the results obtained from cell fusion index have shown the ability of BeWo b30 to fuse. This is significant as cell differentiation from cytotrophoblast to syncytiotrophoblast is a key feature of the human placental barrier allowing the regulation of drug and nutrient transport [2]. This section of the report validates the integrity of the barrier which will be reflected in the impedance spectroscopy measurements.

3.2 Electrical Properties of BeWo b30 Monolayer

3.2.1 Trans-epithelial Electrical Resistance

As a first approach, stainless steel electrodes were utilized to measure cell impedance and extract the TEER value. Figure 3.4 shows the TEER measurement for the control well using stainless steel electrodes. As can be seen, the measurements are not consistent with the literature measurements. The values of the measurements are expected to increase; however, they fluctuate and are not stable although a confluent monolayer was observed at Day 4. Therefore, the next sets of measurements were performed using the STX4 electrodes.

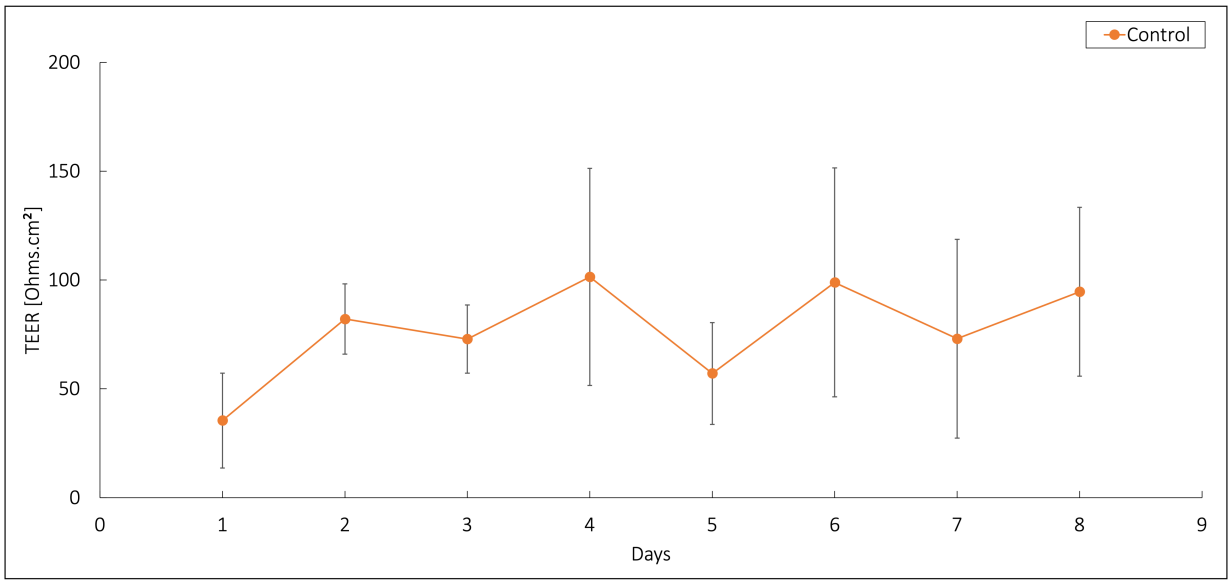

Figure 3.4: BeWo b30 TEER measurements using stainless steel electrodes.

Table 3.3 and Table 3.4 provide the specific electrical resistance values with standard deviation for uncoated and collagen coated transwell membranes, respectively, at various days in culture post-seeding. The data in the tables includes results with and without the

addition of 20 μM of forskolin. Additionally, Figure 3.5 displays the electrical resistance of cell junctions for uncoated transwell membranes, while Figure 3.7 represents the electrical resistance for collagen coated transwell membranes. Both figures show the resistance development over the days in culture after cell seeding.

Table 3.3: TEER [Ωcm^2] measurements for uncoated transwell membranes

	Day 1	Day 2	Day 3	Day 4	Day 5	Day 6	Day 7
Control	5.23	6.99	9.99	23.64	21.72	27.46	25.16
	±3.39	±5.85	±2.61	±3.70	±11.12	±9.77	±17.77
+20 μM	6.19	9.42	8.81	13.90	8.86	6.90	6.50
forskolin	±2.43	±4.21	±3.11	±2.89	±3.27	±1.17	±1.93

Values are Means ±SD; average n = 9. Transepithelial electrical resistance measurements corrected for background values.

Table 3.4: TEER [Ωcm^2] measurements over seven day period for coated transwell membranes

	Day 1	Day 2	Day 3	Day 4	Day 5	Day 6	Day 7
Control	2.94	2.87	5.00	6.58	8.14	12.56	13.89
	±0.20	±0.96	±0.46	±0.28	±1.15	±0.67	±0.68
+20 μM	4.42	4.97	6.71	15.07	15.84	15.51	15.57
forskolin	±0.35	±0.04	±1.08	±0.94	±1.28	±1.94	±0.59

Values are Means ±SD; average n = 9. Transepithelial electrical resistance measurements corrected for background values.

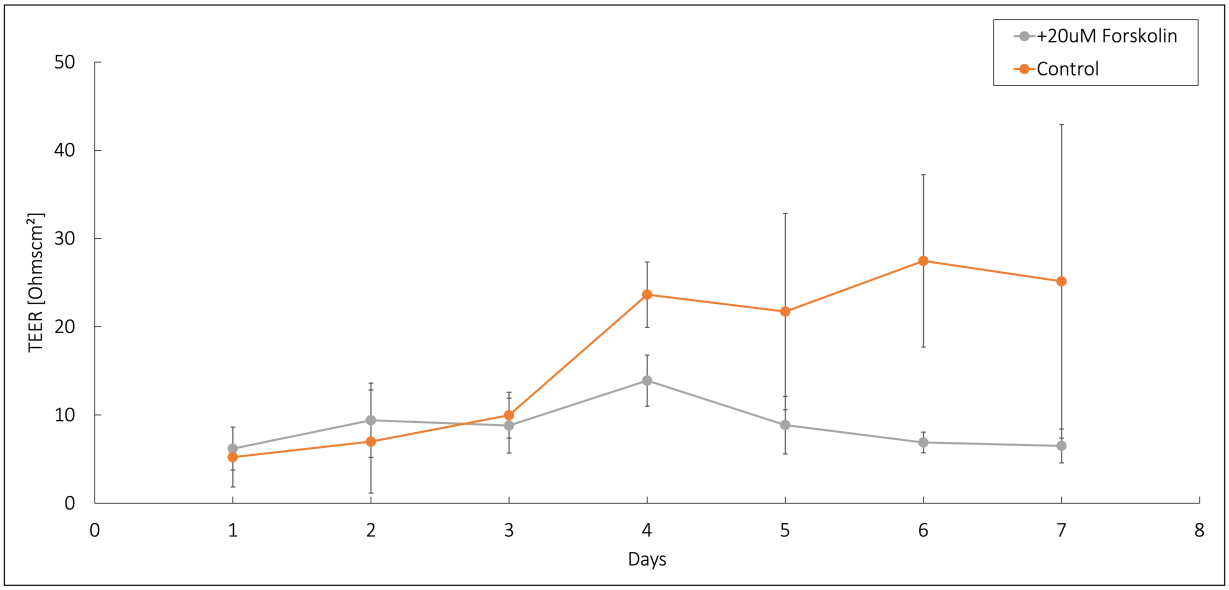

Figure 3.5: BeWo b30 TEER measurements for uncoated transwell membrane

Monolayer cultures with (grey) and without (orange) forskolin. Data represent Means ±SD from triplicate samples (n = 9).

Figure 3.5 illustrates the contrasting trends observed in the Control group and the 20 μM forskolin treated group during the experiment. The Control group shows a progressive increase in the response over the course of the experiment. In contrast, the group treated with 20 μM forskolin shows a slight initial increase followed by a decrease in the response over time. The overall mean TEER values are higher for the control samples. The error bar represents the standard deviation of triplicate samples. In fact, the error from samples is two times higher than the error from the fitting algorithm which is negligible as can be seen in Appendix 4.

As shown in Hohn et al.'s work, BeWo cell lines exhibit poor cell attachment to uncoated substrate [43]. The decrease in TEER values for forskolin treated samples measured on Day 5, Day 6 and Day 7 can be attributed to cell detachment, as illustrated in Figure 3.6.

Morevoer, the control uncoated group exhibits more variability in the data, particularly on Day 5, Day 6, and Day 7 suggesting that variability of cell growth on the substrates are affected by the surface.

Therefore, it was concluded that for better cell attachment and improved measurements, Collagen Type I was used to coat the substrate and allow for better cell adhesion.

In the initial phase of the study, a statistical analysis was performed to assess whether the application of a coating on the insert had any significant impact on resistance measurements. A paired samples T-test was conducted to compare the resistance measurements between the coated and uncoated blanks. The results of this analysis are presented in Table 3.5. The obtained p-value, which is greater than 0.05, indicates that there is no statistically significant difference between the coated and uncoated blanks concerning the electrical resistance. Based on this finding, we can confidently conclude that the coating did not influence the TEER measurements. Therefore, any observed changes in TEER are attributed to the cellular elements rather than the presence of the coating.

Table 3.5: Paired Samples T-Test of TEER measurements with (C) and without (NC) collagen on blank wells

Measure 1		Measure 2	t	df	p
C2	-	NC2	0.050	2	0.964
C3	-	NC3	0.060	2	0.958
C4	-	NC4	0.818	2	0.499
C5	-	NC5	0.089	2	0.937
C6	-	NC6	0.555	2	0.635
C7	-	NC7	0.518	2	0.656

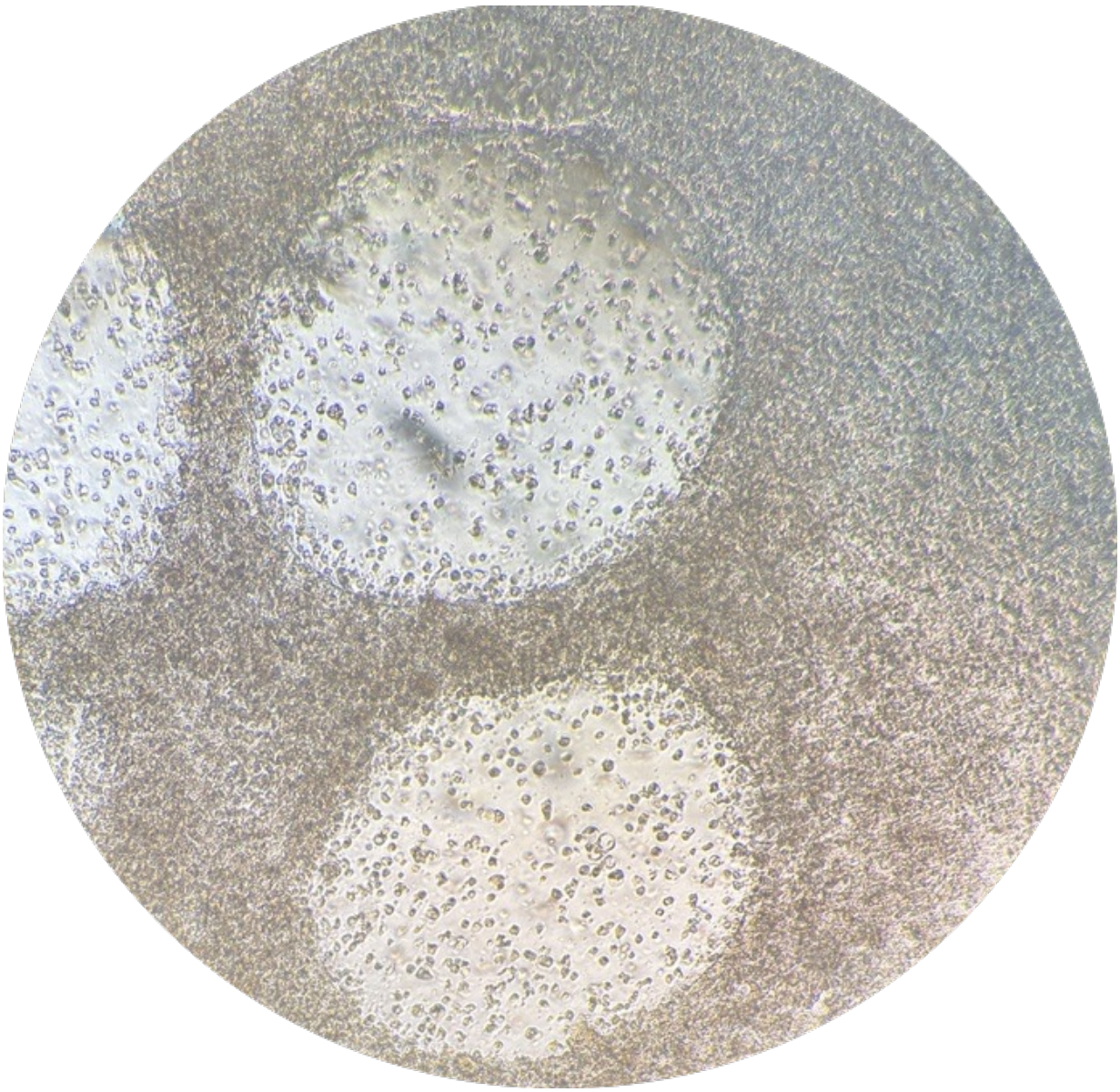

Figure 3.6: BeWo b30 cell detachment observed at Day 5.

Image acquired through the occular of a microscope using a mobile phone.

Figure 3.7 shows the development of TEER by BeWo b30 for Collagen Type I coated transwell substrates. As can be seen, the control group shows a progressive increase in the response over the course of the experiment similar to the control of the uncoated substrate. On the other hand, the samples treated with forskolin show a different trend. TEER remains low before reaching a peak at Day 4, indicating the formation of a confluent monolayer as previously confirmed with immunofluorescence imaging shown in Section 3.1. The TEER value for the treated samples on Day 4 is 3 times higher than untreated samples representing a more electrical current restricted multi-nucleated structure.

As previously mentioned, forskolin treatment reduces cell proliferation. This is reflected in the measurement where TEER values remain constant after the formation of a confluent monolayer formation as opposed to the linearly increasing trend of untreated samples. In addition, given that the cells are attached to the substrate, reflected by the constant TEER values at Day 5, Day 6 and Day 7, the BeWo monolayer retains its integrity. On the other hand, the resistance of the untreated samples remained in an increasing linear trend due to its lack of fusion and multiple layer formation. This can be explained refering back to the immunofluorescence imaging. In fact, the untreated cells express higher E-cadherin protein than treated cells. This indicates the tight junction formation. Moreover, due to its epithelial nature, BeWo b30 cells will start to grow a multi-layer. Therefore, the TEER of untreated cells will continuously increase throughout the days without any cell fusion changes as shown in the previous section. Although TEER values on Day 6 for both treated and untreated are similar, the morphology of the cells are different as was shown in the immunofluorescence images.

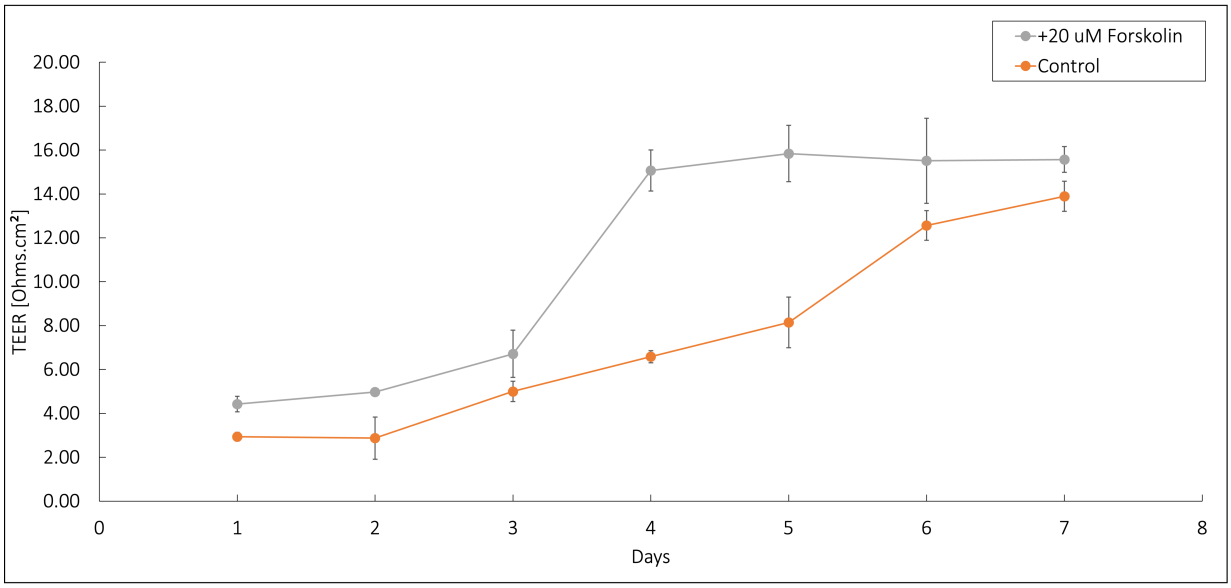

Figure 3.7: BeWo b30 TEER measurements for collagen coated transwell membranes. *Monolayer cultures with (grey) and without (orange) forskolin. Data represent means ±SD from triplicate samples (n = 9).*

A T-test was performed to determine whether there is a statistically significant difference between treated and untreated samples. Table 3.6 shows the p-value comparing samples with (F) and without forskolin (NF) at the different time points starting the day after forskolin addition. It was shown that there is a statistically significant difference between Day 4, Day 5 and Day 7 confirming the effect of forskolin on TEER values as shown in Figure 3.8.

Table 3.6: Paired Samples T-Test of TEER measurements with (F) and without (NF) forskolin on collagen substrate

Measure 1		Measure 2	t	df	p
F3	-	NF3	−0.303	8	0.769
F4	-	NF4	5.335	8	< .01
F5	-	NF5	3.042	8	0.016
F6	-	NF6	−1.085	8	0.310
F7	-	NF7	−2.512	8	0.036

Note. Student's t-test.

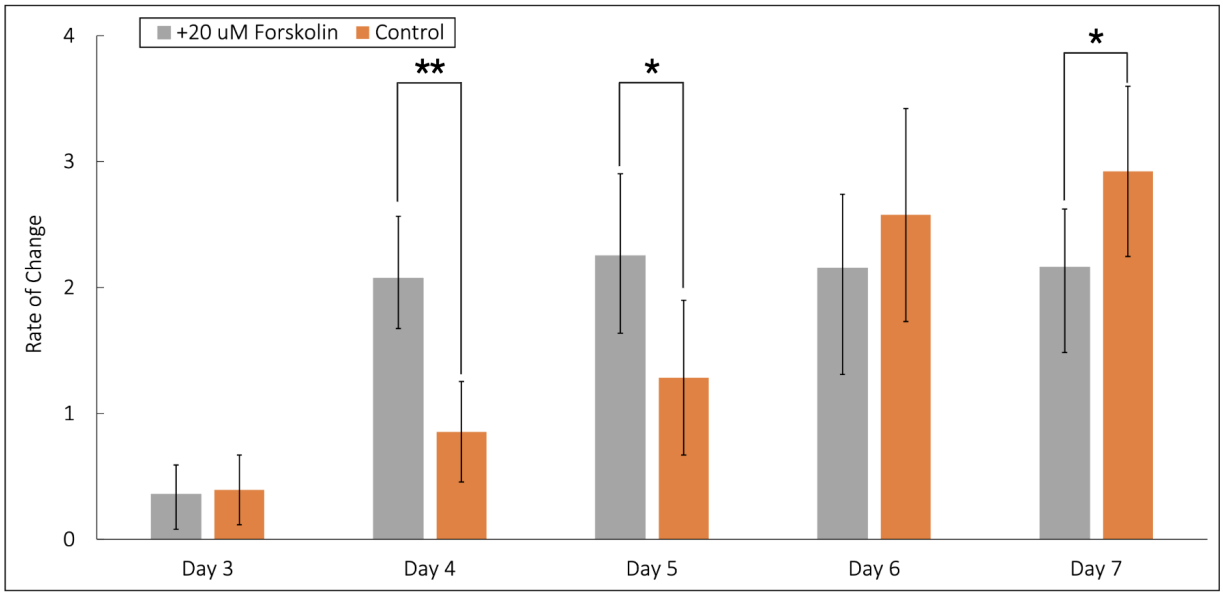

Figure 3.8: Rate of change of TEER with respect to Day 2, forskolin addition. *Monolayer cultures with (grey) and without (orange) forskolin. Data represent Means ±SD from triplicate samples (n = 9). * and ** indicate p < 0.05 and p < 0.01, respectively.*

While the TEER values observed in this system may appear relatively low when compared to findings from other studies, it is crucial to acknowledge that variations in instrumentation, temperature, buffers, growth substrates, and other lab-specific factors could contribute to these discrepancies. However, the trend of the measured values are similar to the findings described in Section 1.5.2 indicating that the measurement device developed in this study is suitable to investigate BeWo b30 barrier integrity for future studies such as co-culture, or the effect of drugs on the placental barrier [29] [19].

3.2.2 Electrical Capacitance Property

Table 3.7 and Table 3.8 provide the specific electrical capacitance values with standard deviation for uncoated and collagen coated transwell membranes, respectively, at various days in culture post-seeding. The data in the tables includes results with and without the addition of 20 μM of forskolin. Additionally, Figure 3.9 displays the electrical capacitance of cell membrane for uncoated transwell membranes, while Figure 3.10 represents the electrical capacitance for collagen coated transwell membranes. Both figures show the capacitance development over the days in culture after cell seeding.

Table 3.7: Capacitance [μFcm^2] measurements over seven day period for uncoated transwell inserts.

	Day 1	Day 2	Day 3	Day 4	Day 5	Day 6	Day 7
Control	0.65	0.56	0.83	2.35	1.91	1.57	0.54
	±0.49	±0.24	±0.08	±1.26	±1.12	±0.24	±0.21
+20 μM	1.10	0.73	0.75	0.75	0.87	0.80	0.44
forskolin	±0.08	±0.04	±0.03	±0.00	±0.06	±0.02	±0.10

Values are Means ±SD; average n = 9. Cell capacitance measurements.

Table 3.8: Capacitance [μFcm^2] measurements over seven day period for coated transwell inserts.

	Day 1	Day 2	Day 3	Day 4	Day 5	Day 6	Day 7
Control	1.32	0.67	0.51	1.05	1.32	1.42	1.55
	$\pm$0.16	$\pm$0.12	$\pm$0.10	$\pm$0.01	$\pm$0.06	$\pm$0.04	$\pm$0.07
+20 μM	0.60	0.86	0.90	1.09	1.06	1.01	0.86
forskolin	$\pm$0.23	$\pm$0.19	$\pm$0.19	$\pm$0.11	$\pm$0.06	$\pm$0.12	$\pm$0.15

Values are Means $\pm$SD; average n = 9. Cell capacitance measurements.

As can be seen on Figure 3.9, the cell membrane capacitance for the control group increases gradually from Day 1 and reaches a peak value of 1.91 μFcm^2. There is a decreasing trend after Day 4 with large variation for the different samples. On the other hand, the forskolin treated samples have an overall decreasing trend since Day 1 with small deviations. However, as mentioned previously, detachment occurred at Day 5; therefore, it is not possible to draw any conclusions from this set of measurement.

Figure 3.10 shows the capacitance of the cell membrane for collagen coated substrate. The results show a decrease from Day 1 to Day 3 for the control group. However, the capacitance starts to increase from Day 4, when a monolayer forms. The change post confluency suggest an increasing trend with small variations between samples. On the other hand, the electrical capacitance of forskolin treated sample show a slight increasing trend from Day 1 to Day 4 followed by a decrease. As mentioned in Section 1.5.4, the electrical capacitance is cell dependant. Figure 3.10 shows that the cell capacitance for control wells increases throughout the days. However, it decreases for forskolin treated samples. We hypothesis that This phenomenon can be associated with a decrease in cell surface area. When BeWo b30 cells undergo differentiation and start to fuse, the nuclei

area increases as shown in Blundel et. al. where BeWo b30 nuclei area increases from about 1000 pixels at 24 h to 1500 pixels at 72 h [2]. This suggests a decrease in cell membrane surface area, compared to unfused cells, resulting in a decrease in electrical capacitance. On the other hand, due to the multiple layer formation for the control group, the overall membrane surface area will increase. This phenomenon will result in an increase of the electrical capacitance.

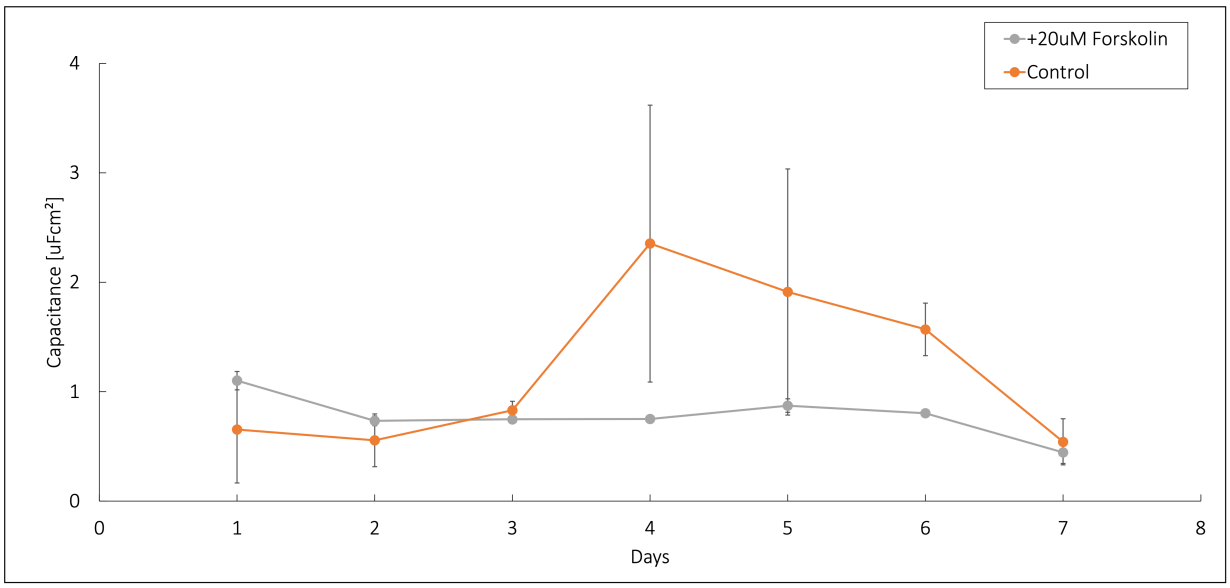

Figure 3.9: BeWo b30 electrical capacitance development for uncoated transwells. *Monolayer cultures with (blue) and without (orange) forskolin. Data represent means ±SD from triplicate samples.*

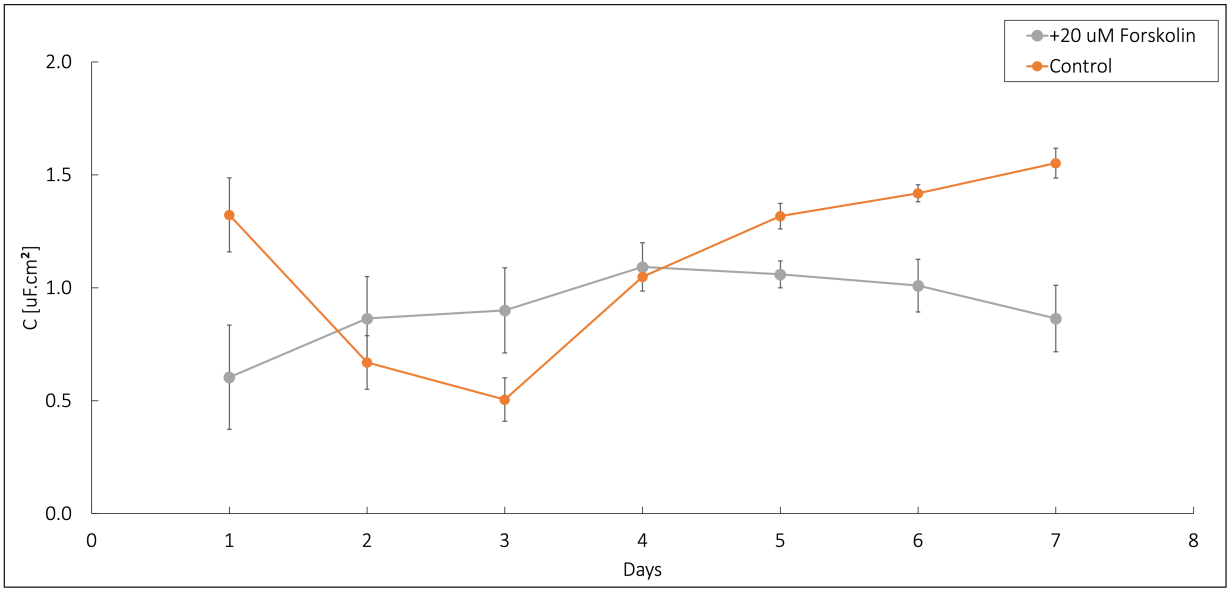

Figure 3.10: BeWo b30 electrical capacitance development for coated transwells. *Monolayer cultures with (blue) and without (orange) forskolin. Data represent means ±SD from triplicate samples.*

A paired T-test was performed to determine whether there is a statistically significant difference between the electrical capacitance of forskolin treated and control groups. Figure 3.11 shows the rate of change of electrical capacitance with respect to Day 2. As can be seen there is a statistically significant difference at Day 3 which can be associated with the difference of the monolayer formation. In addition, a statistically significant difference exist at Day 5, Day 6 and Day 7 where peak fusion occurs. This confirms a difference in the electrical capacitance measurements caused by forskolin.

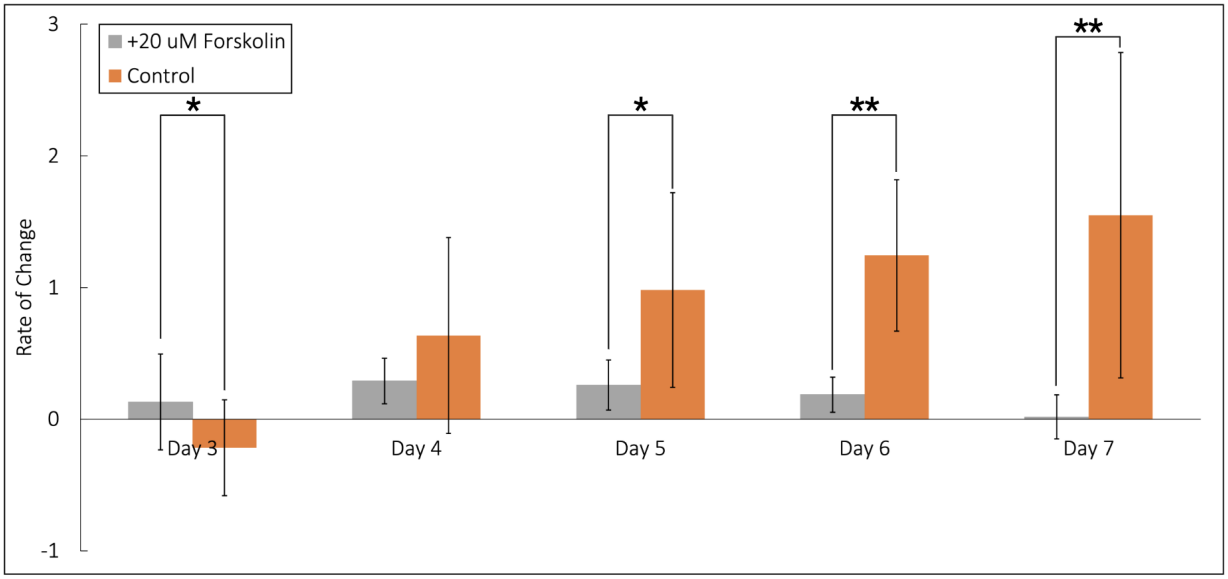

Figure 3.11: Rate of change of capacitance with respect to Day 2, forskolin addition. *Monolayer cultures with (grey) and without (orange) forskolin. Data represent Means ±SD from triplicate samples ($n = 9$). * and ** indicate $p < 0.05$ and $p < 0.01$, respectively.*

3.3 Preliminary Placenta-on-a-chip Results

3.3.1 Cell Culture on Chip

An initial design and fabrication of a microfluidic chip was completed on an international research visit at Université Montpellier (France). To test this chip, HUVECs were chosen as the cell model as they have been previously reported to be able to form a uniform monolayer with cell-cell junction allowing the use of impedance spectroscopy to measure TEER and cell capacitance [47]. Moreover, the placenta model, as explained previously, is a multi-layer structure composed of both the fetus and the mother cells, separated by a thin interstitium. Therefore, to more precisely mimic and model the placenta, the presence of HUVECs are necessary in co-culture with BeWo b30 [24]. Hence, this validation step ensures that the microfluidic chip functions effectively in a co-culture setup, where it can support both the HUVECs and BeWo b30 cells in a manner that closely resembles the intricate multi-layer composition of the placenta.

Figure 3.12 shows the HUVEC cells at 4-hours post-seeding (Panel A) and Day 1 (Panel B) in microfluidic culture. Successful attachment and growth can be seen on the membrane of the microfluidic chip. However, when air bubbles were introduced during media replenishment, they caused significant cell death. This was due to the mechanical stress of a circulating bubble and flow blockage, which reduced nutrient supply to cells [48]. Upon investigation, it was determined that there was incomplete sealing of the inlet and outlet on the chip which should be mended for future designs. Though this defect prevents further investigation on this chip, these preliminary results indicate that this design and fabrication approach results in a platform that can be employed in a variety of applications and, within the context of this study, its use of impedance spectroscopy.

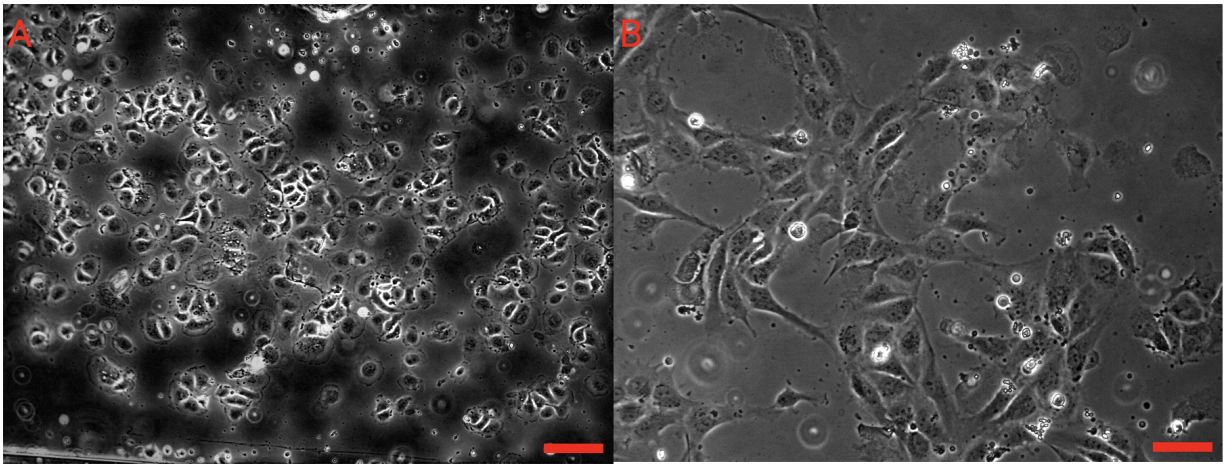

Figure 3.12: HUVEC cells in microfluidic chip

A) 4-hours post-seeding and B) Day 1. Scale bar: 55 µm.

3.3.2 Impedance Spectroscopy

The microchip underwent perfusion with PBS 1x, followed by impedance measurements. The impedance of PBS was measured using the assembled chip system. The obtained data was used to generate the Nyquist plot, characterising the real and imaginary parts on a cartesian coordinate system [45]. In fact, without the presence of the cells and given a double layer capacitance property developed by the electrodes and the solution, the theoretical Nyquist plot can be seen in Figure 3.13 [37] [45]. As anticipated the measured impedance from the chip and the corresponding Nyquist plot, depicted in Figure 3.14, reflects a combination of resistance and capacitance arranged in parallel to model the gold electrode, with an additional media resistance introduced by the PBS. Upon analysis using ZView software, the electrode's resistance was estimated to be approximately 164.5 kΩ. However, the presence of a thick layer of silver coating on the electrodes, to establish the electrical connection, resulted in a considerable increase in resistance, potentially impacting the overall accuracy of measurements when cells are introduced to the chip. Therefore,

there is a need to identify an alternative solution to mitigate the effects of the silver coating. One viable approach is the implementation of wire bonding or silver paste.

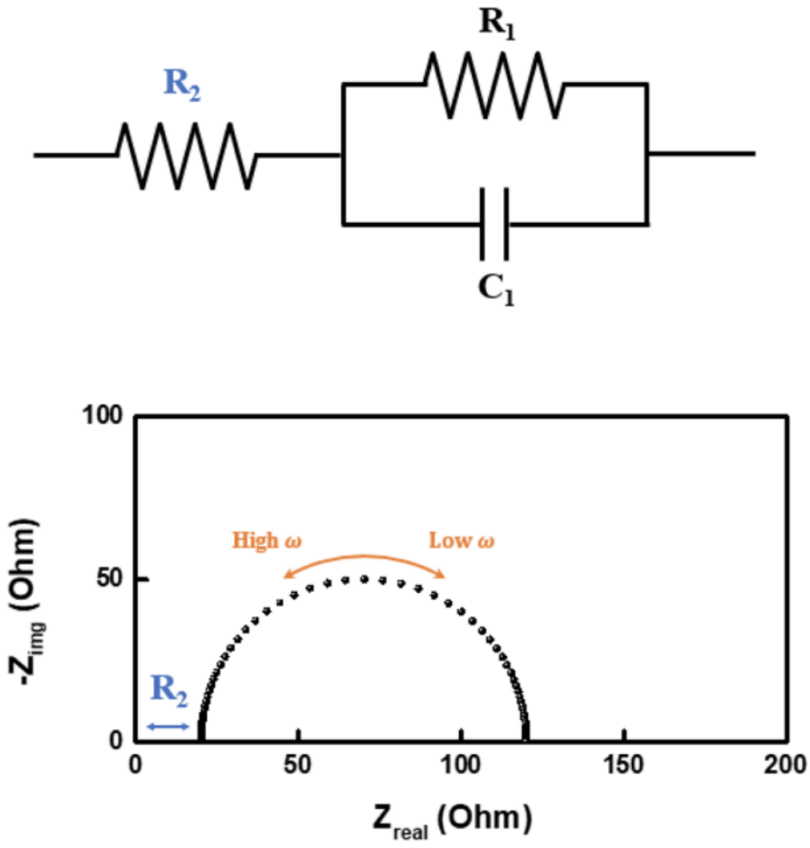

Figure 3.13: Bioimpedance of electrode in solution.

a) Equivalent electrical model for double layer capacitance, C_1 *is the capacitance of the electrode,* R_1 *is resistance of the electrode,* R_2 *is the resistance of the solution. b) Theoretical Nyquist plot of the double layer capacitance.*

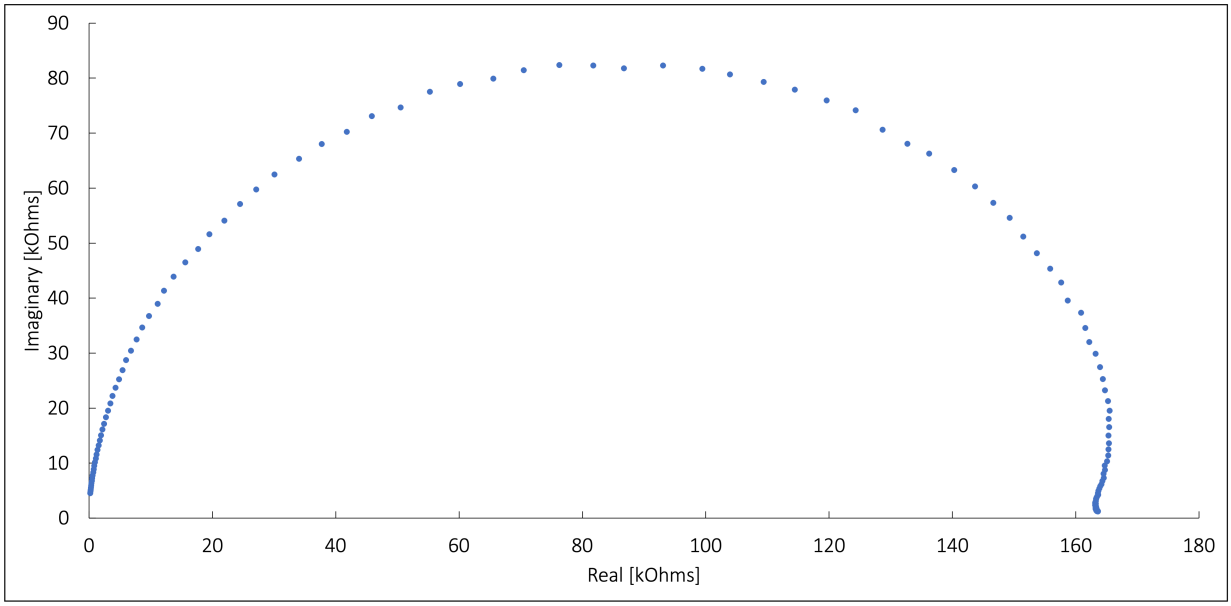

Figure 3.14: Nyquist plot of PBS 1x perfused chip.

Chapter 4

Conclusion

The major aims of our research were to: (1) Design and optimize a low cost, effective and reproducible impedance measuring device to assess the placenta barrier permeability changes, (2) Measure and track electrical properties (resistivity and capacitivity) of a monolayer of epithelial cells (BeWo) to validate the setup, (3) Capture and process syncytialisation data from TEER to correlate with the cell fusion index obtained from immunofluorescence imaging and (4) Propose a Lab-on-a-Chip (LOC) design to mimic a physiological placental barrier in vitro.

We showed that the AD2 device can be used to measure and track the placenta barrier permeability changes, namely TEER and capacitive properties of the BeWo b30 cell line. When seeded on collagen treated transwells inserts, BeWo b30 were able to grow a confluent monolayer in four days. This was reflected in immunofluorescence imaging. However, by staining the cells, this method renders the cell unusable for further studies. Hence, the use of TEER allows to track and measure the cells' barrier permeability without hindering the cells. Therefore, to prove the effectiveness and reproducibility of our system, BeWo b30 triplicate samples were seeding on collagen coated transwell inserts and treated with

forskolin to measure the cells' impedance for seven days and compare the measured trend with the cell fusion index obtained from immunofluorescene imaging.

It was first concluded using immunofluorescence imaging that the cell fusion index of BeWo b30 treated cells increased 5 times compared to untreated samples at Day 4. This shows that forskolin treated samples induces differentiation of BeWo b30, a key factor mimicking the morphology of syncytialized primary culture.

Second, the impedance spectroscopy measurement confirmed the formation of a confluent monolayer and the integrity of the cell layer. In fact, TEER remained constant through Day 1 to Day 3 for both treated and untreated samples. The electrical resistance tripled for treated samples showing the formation of a confluent layer. Thereafter, this resistance remained constant for treated samples reflecting the intact cell barrier and retention of the barrier's integrity over the next 3 days. On the other hand, the resistance of the untreated samples remained in an increasing linear trend due to its lack of fusion and multiple layer formation. This method allowed to monitor the BeWo b30 barrier integrity without hindering the cell function as opposed to immunofluorescent imaging.

Finally, the electrical capacitance of BeWo b30 was measured. The cell capacitance is an electrical property dependant on the cell membrane surface area. The measurements show that at Day 4, at the formation of a confluent monolayer, the electrical capacitance of the cells decreases for treated sample as opposed to untreated samples. This reflects that the surface area of the BeWo b30 cells decreases when the samples were treated with forskolin.

The development of the microfluidic chip with integrated electrodes was finalized; however, there remains a testing phase with impedance spectroscopy and immunofluorescence imaging in order to compare the obtained results with the results measured from the transwells.

References

[1] R. Alicki, D. Gelbwaser-Klimovsky, and A. Jenkins, "Leaking elastic capacitor as model for active matter," *Physical Review E*, vol. 103, May 2021.

[2] C. Blundell, E. R. Tess, A. S. Schanzer, C. Coutifaris, E. J. Su, S. Parry, and D. Huh, "A microphysiological model of the human placental barrier," *Lab on a Chip*, vol. 16, no. 16, p. 3065–3073, 2016.

[3] G. J. Burton and A. L. Fowden, "The placenta: A multifaceted, transient organ," *Philosophical Transactions of the Royal Society B: Biological Sciences*, vol. 370, no. 1663, p. 20140066, 2015.

[4] M. Rothbauer, N. Patel, H. Gondola, M. Siwetz, B. Huppertz, and P. Ertl, "A comparative study of five physiological key parameters between four different human trophoblast-derived cell lines," *Scientific Reports*, vol. 7, no. 1, 2017.

[5] R. L. Pemathilaka, J. D. Caplin, S. S. Aykar, R. Montazami, and N. N. Hashemi, "Placenta-on-a-chip: Placenta-on-a-chip: In vitro study of caffeine transport across placental barrier using liquid chromatography mass spectrometry (global challenges 3/2019)," *Global Challenges*, vol. 3, no. 3, p. 1970031, 2019.

[6] M. K. Wong, *The Design and Characterisation of Microphysiological Platforms to Model the Human Placenta*. PhD thesis, 2020.

[7] R. L. Pemathilaka, D. E. Reynolds, and N. N. Hashemi, "Drug transport across the human placenta: Review of placenta-on-a-chip and previous approaches," *Interface Focus*, vol. 9, no. 5, p. 20190031, 2019.

[8] E. Bongaerts, L. Aengenheister, B. B. Dugershaw, P. Manser, M. B. Roeffaers, M. Ameloot, T. S. Nawrot, H. Bové, and T. Buerki-Thurnherr, "Label-free detection of uptake, accumulation, and translocation of diesel exhaust particles in ex vivo perfused human placenta," *Journal of Nanobiotechnology*, vol. 19, no. 1, 2021.

[9] S. K. Griffiths and J. P. Campbell, "Placental structure, function and drug transfer," *Continuing Education in Anaesthesia Critical Care amp; Pain*, vol. 15, no. 2, p. 84–89, 2015.

[10] B. Editors, "Placenta - what is it and how it works," Jul 2017.

[11] P. Díaz, T. L. Powell, and T. Jansson, "The role of placental nutrient sensing in maternal-fetal resource allocation1," *Biology of Reproduction*, vol. 91, no. 4, 2014.

[12] J. Guibourdenche, T. Fournier, A. MalassinĂŠŠ, and D. Evain-Brion, "Development and hormonal functions of the human placenta.," *Folia Histochemica et Cytobiologica*, vol. 47, no. 5, 2010.

[13] E. Delorme-Axford, Y. Sadovsky, and C. B. Coyne, "The placenta as a barrier to viral infections," *Annual Review of Virology*, vol. 1, no. 1, p. 133–146, 2014.

[14] F. A. Elzinga, B. Khalili, D. J. Touw, J. R. Prins, P. Olinga, H. G. Leuvenink, H. van Goor, S. J. Gordijn, A. Nagelkerke, and P. Mian, "Placenta-on-a-chip as an in

vitro approach to evaluate the physiological and structural characteristics of the human placental barrier upon drug exposure: A systematic review," *Journal of Clinical Medicine*, vol. 12, no. 13, p. 4315, 2023.

[15] P. Calis, L. Vojtech, F. Hladik, and M. G. Gravett, "A review of ex vivo placental perfusion models: An underutilized but promising method to study maternal-fetal interactions," *The Journal of Maternal-Fetal amp; Neonatal Medicine*, vol. 35, no. 25, p. 8823–8835, 2021.

[16] Y. Pu, J. Gingrich, and A. Veiga-Lopez, "A 3-dimensional microfluidic platform for modeling human extravillous trophoblast invasion and toxicological screening," *Lab on a Chip*, vol. 21, no. 3, p. 546–557, 2021.

[17] F. Yin, Y. Zhu, M. Zhang, H. Yu, W. Chen, and J. Qin, "A 3d human placenta-on-a-chip model to probe nanoparticle exposure at the placental barrier," *Toxicology in Vitro*, vol. 54, p. 105–113, 2019.

[18] B. Mosavati, A. Oleinikov, and E. Du, "3d microfluidics-assisted modeling of glucose transport in placental malaria," *Scientific Reports*, vol. 12, no. 1, 2022.

[19] F. Liu, M. J. Soares, and K. L. Audus, "Permeability properties of monolayers of the human trophoblast cell line bewo," *American Journal of Physiology-Cell Physiology*, vol. 273, no. 5, 1997.

[20] R. A. Pattillo, G. O. Gey, E. Delfs, and R. F. Mattingly, "Human hormone production in vitro," *Science*, vol. 159, no. 3822, p. 1467–1469, 1968.

[21] K. Orendi, M. Gauster, G. Moser, H. Meiri, and B. Huppertz, "The choriocarcinoma cell line bewo: Syncytial fusion and expression of syncytium-specific proteins," *REPRODUCTION*, vol. 140, no. 5, p. 759–766, 2010.

[22] J. Liu, O. Chesnokova, I. Oleinikov, Y. Qiang, A. V. Oleinikov, and E. Du, "Optimization of in vitro trophoblast assay for real-time impedimetric sensing of trophoblast-erythrocyte interactions in plasmodium falciparum malaria," *Analytical and Bioanalytical Chemistry*, vol. 412, no. 16, p. 3915–3923, 2020.

[23] S. Al-Nasiry, B. Spitz, M. Hanssens, C. Luyten, and R. Pijnenborg, "Differential effects of inducers of syncytialization and apoptosis on bewo and jeg-3 choriocarcinoma cells," *Human Reproduction*, vol. 21, no. 1, p. 193–201, 2005.

[24] G. Rabussier, I. Bünter, J. Bouwhuis, C. Soragni, T. van Zijp, C. P. Ng, K. Domansky, L. J. de Windt, P. Vulto, C. E. Murdoch, and et al., "Healthy and diseased placental barrier on-a-chip models suitable for standardized studies," *Acta Biomaterialia*, vol. 164, p. 363–376, 2023.

[25] I. Lang, M. A. Pabst, U. Hiden, A. Blaschitz, G. Dohr, T. Hahn, and G. Desoye, "Heterogeneity of microvascular endothelial cells isolated from human term placenta and macrovascular umbilical vein endothelial cells," *European Journal of Cell Biology*, vol. 82, no. 4, p. 163–173, 2003.

[26] M. K. Wong, E. W. Li, M. Adam, P. R. Selvaganapathy, and S. Raha, "Establishment of an in vitro placental barrier model cultured under physiologically relevant oxygen levels," *Molecular Human Reproduction*, vol. 26, no. 5, p. 353–365, 2020.

[27] C. Azar, M. C. Valentine, J. Trausch-Azar, L. Rois, M. Mahjoub, D. M. Nelson, and A. L. Schwartz, "Rna-seq identifies genes whose proteins are upregulated during syncytia development in murine c2c12 myoblasts and human bewo trophoblasts," *Physiological Reports*, vol. 9, no. 1, 2021.

[28] H. Matsukawa, M. Ikezaki, K. Nishioka, N. Iwahashi, M. Fujimoto, K. Nishitsuji, Y. Ihara, and K. Ino, "Calnexin is involved in forskolin-induced syncytialization in cytotrophoblast model bewo cells," *Biomolecules*, vol. 12, no. 8, p. 1050, 2022.

[29] B. Srinivasan, A. R. Kolli, M. B. Esch, H. E. Abaci, M. L. Shuler, and J. J. Hickman, "Teer measurement techniques for in vitro barrier model systems," *SLAS Technology*, vol. 20, no. 2, p. 107–126, 2015.

[30] E. Ferrari, C. Palma, S. Vesentini, P. Occhetta, and M. Rasponi, "Integrating biosensors in organs-on-chip devices: A perspective on current strategies to monitor microphysiological systems," *Biosensors*, vol. 10, no. 9, p. 110, 2020.

[31] A. Nicolas, F. Schavemaker, K. Kosim, D. Kurek, M. Haarmans, M. Bulst, K. Lee, S. Wegner, T. Hankemeier, J. Joore, and et al., "High throughput transepithelial electrical resistance (teer) measurements on perfused membrane-free epithelia," *Lab on a Chip*, vol. 21, no. 9, p. 1676–1685, 2021.

[32] H. Tang, Z. Jiang, H. He, X. Li, H. Hu, N. Zhang, Y. Dai, and Z. Zhou, "Uptake and transport of pullulan acetate nanoparticles in the bewo b30 placental barrier cell model," *International Journal of Nanomedicine*, vol. Volume 13, p. 4073–4082, 2018.

[33] H. Liu, F. Shi, X. Tang, S. Zheng, J. Kolb, and C. Yao, "Application of bioimpedance spectroscopy to characterize chemoresistant tumor cell selectivity of nanosecond pulse stimulation," *Bioelectrochemistry*, vol. 135, p. 107570, 2020.

[34] M. Amini, J. Hisdal, and H. Kalvøy, "Applications of bioimpedance measurement techniques in tissue engineering," *Journal of Electrical Bioimpedance*, vol. 9, no. 1, p. 142–158, 2018.

[35] K. Benson, S. Cramer, and H.-J. Galla, "Impedance-based cell monitoring: Barrier properties and beyond," *Fluids and Barriers of the CNS*, vol. 10, no. 1, 2013.

[36] G. Linz, S. Djeljadini, L. Steinbeck, G. Köse, F. Kiessling, and M. Wessling, "Cell barrier characterization in transwell inserts by electrical impedance spectroscopy," *Biosensors and Bioelectronics*, vol. 165, p. 112345, 2020.

[37] J. P. Vigh, A. Kincses, B. Ozgür, F. R. Walter, A. R. Santa-Maria, S. Valkai, M. Vastag, W. Neuhaus, B. Brodin, A. Dér, and et al., "Transendothelial electrical resistance measurement across the blood–brain barrier: A critical review of methods," *Micromachines*, vol. 12, no. 6, p. 685, 2021.

[38] H. Schwan, "Electrical properties of tissues and cell suspensions: Mechanisms and models," *Proceedings of 16th Annual International Conference of the IEEE Engineering in Medicine and Biology Society*, 2002.

[39] J. Fernandes, N. Karra, J. Bowring, R. Reale, J. James, C. Blume, T. J. Pell, W. C. Rowan, D. E. Davies, E. J. Swindle, and et al., "Real-time monitoring of epithelial barrier function by impedance spectroscopy in a microfluidic platform," *Lab on a Chip*, vol. 22, no. 10, p. 2041–2054, 2022.

[40] L. F. Blume, M. Denker, F. Gieseler, and T. Kunze, "Temperature corrected transepithelial electrical resistance (teer) measurement to quantify rapid changes in paracellular permeability," *Pharmazie*, vol. 65, p. 19–24, 2010.

[41] R. D. Simmons, S. Kumar, S. R. Thabet, S. Sur, and H. Jo, "Omics-based approaches to understand mechanosensitive endothelial biology and atherosclerosis," *WIREs Mechanisms of Disease*, vol. 8, p. 378–401, 2016.

[42] Y. Shi, J. Qian, Q. Zhang, Y. Hu, D. Sun, and L. Jiang, "Advanced glycation end products increased placental vascular permeability of human bewo cells via rage/nf-kb signaling pathway," 2020.

[43] H.-P. Hohn, L. R. Boots, H.-W. Denker, and M. Höök, "Differentiation of human trophoblast cells in vitro stimulated by extracellular matrix," *Placenta*, vol. 14, p. 181–200, 1993.

[44] S. Bhansali and A. Vasudev, *MEMS manufacturing techniques for tissue scaffolding devices*. Woodhead Pub., 2012.

[45] W. Choi, H.-C. Shin, J. M. Kim, J.-Y. Choi, and W.-S. Yoon, "Modeling and applications of electrochemical impedance spectroscopy (eis) for lithium-ion batteries," *Journal of Electrochemical Science and Technology*, vol. 11, no. 1, p. 1–13, 2020.

[46] R. Wang, Y.-L. Dang, R. Zheng, Y. Li, W. Li, X. Lu, L.-J. Wang, C. Zhu, H.-Y. Lin, and H. Wang, "Live cell imaging of in vitro human trophoblast syncytialization1," *Biology of Reproduction*, vol. 90, Jun 2014.

[47] M. McRae, L. M. LaFratta, B. M. Nguyen, J. J. Paris, K. F. Hauser, and D. E. Conway, "Characterization of cell-cell junction changes associated with the formation of a strong endothelial barrier," *Tissue Barriers*, vol. 6, no. 1, 2018.

[48] *Nature Reviews Methods Primers*, vol. 2, no. 1, 2022.

APPENDICES

Appendix A: Cell Count Sample

Images aquired through immunofluorescent imaging were analysed first through CellProfiler pipeline and run through QuPath to manually count the missed cells.

1. Smoothing of the images

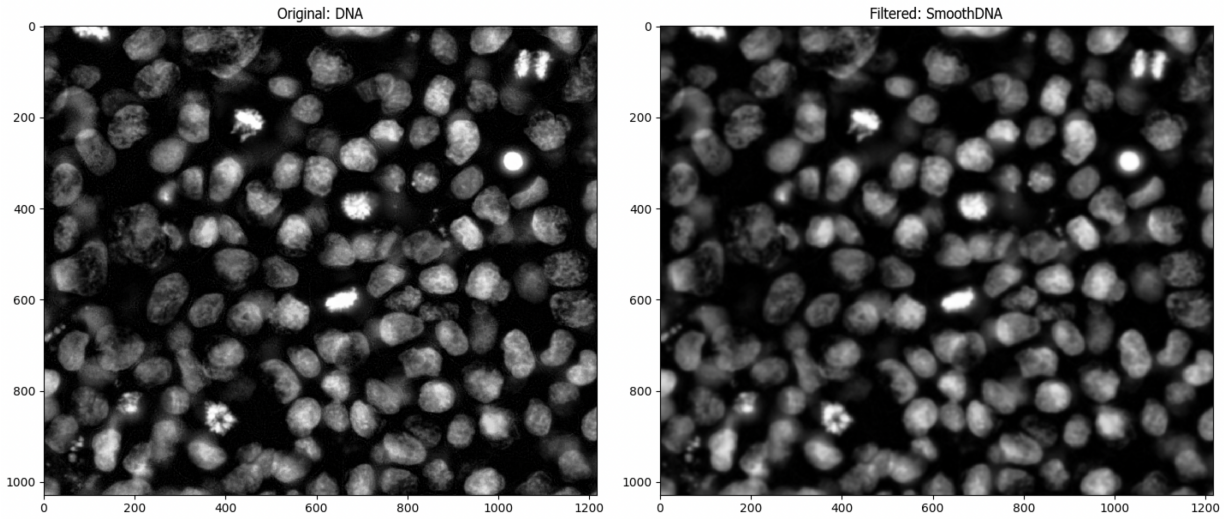

Image smoothing.

2. Identifying primary object, i.e. cell nuclei

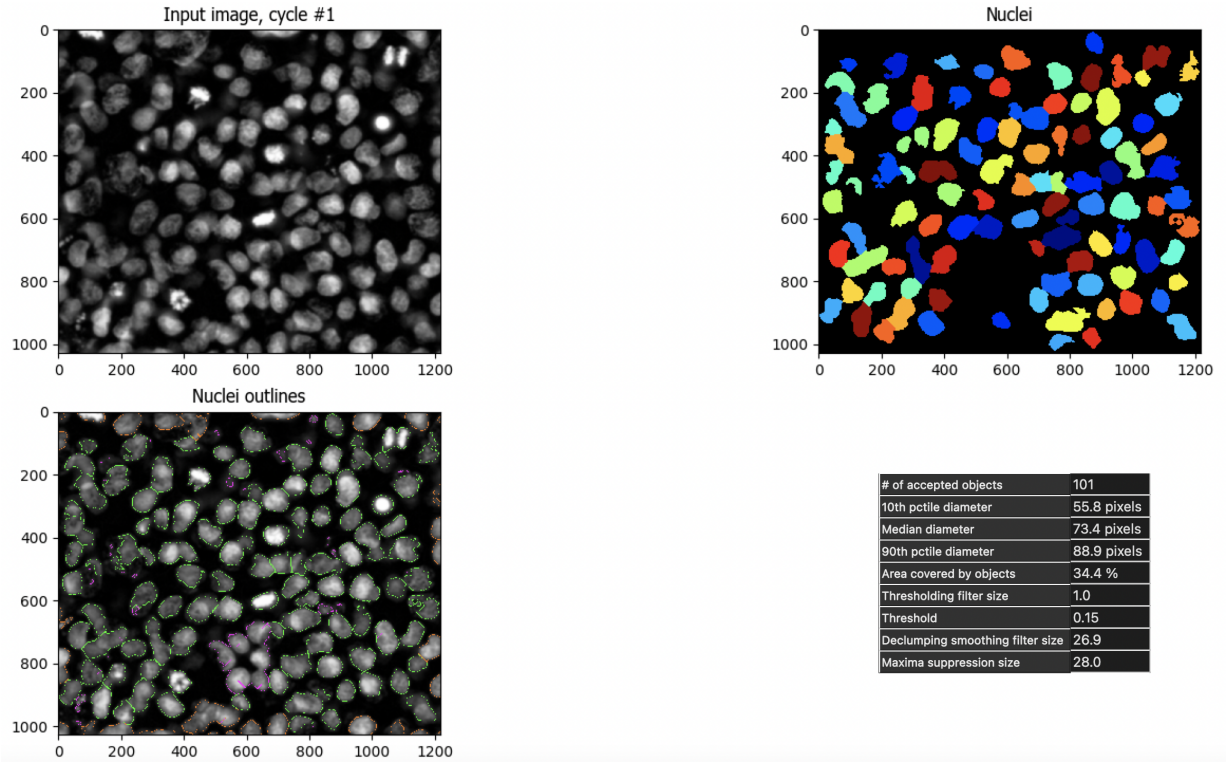

# of accepted objects	101
10th pctile diameter	55.8 pixels
Median diameter	73.4 pixels
90th pctile diameter	88.9 pixels
Area covered by objects	34.4 %
Thresholding filter size	1.0
Threshold	0.15
Declumping smoothing filter size	26.9
Maxima suppression size	28.0

Cell counting.

3. Overlay of the object

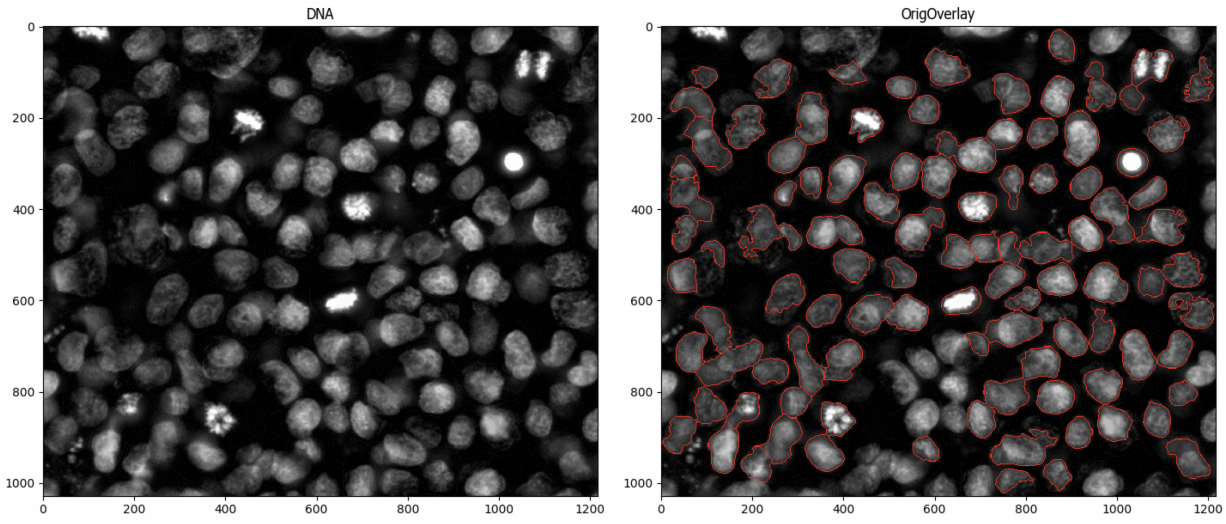

Image overlay.

4. QuPath to manually count the missed nuclei

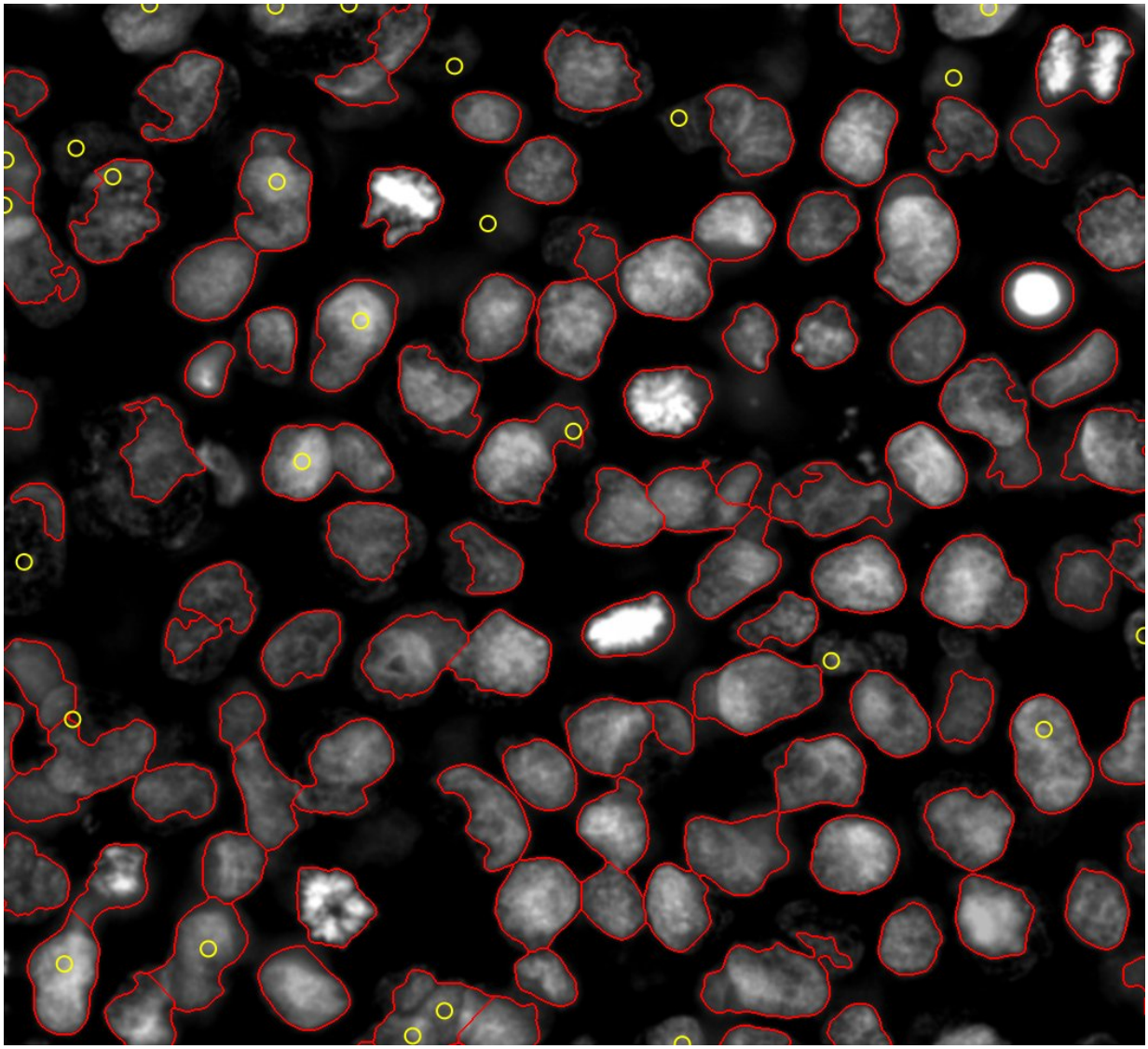

QuPath and final count.

Appendix B: 3D printed support

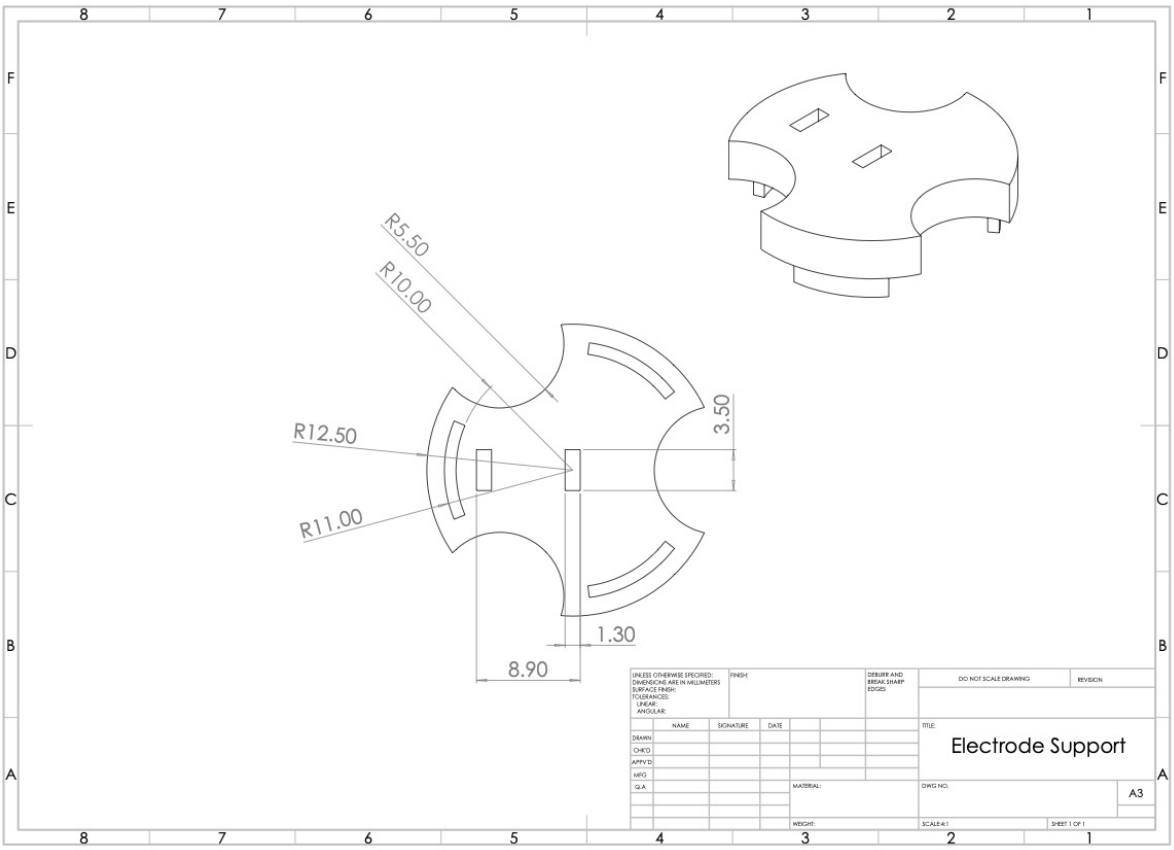

Electrode support.

Measurements in mm

Appendix C: Example of Fit with ZView

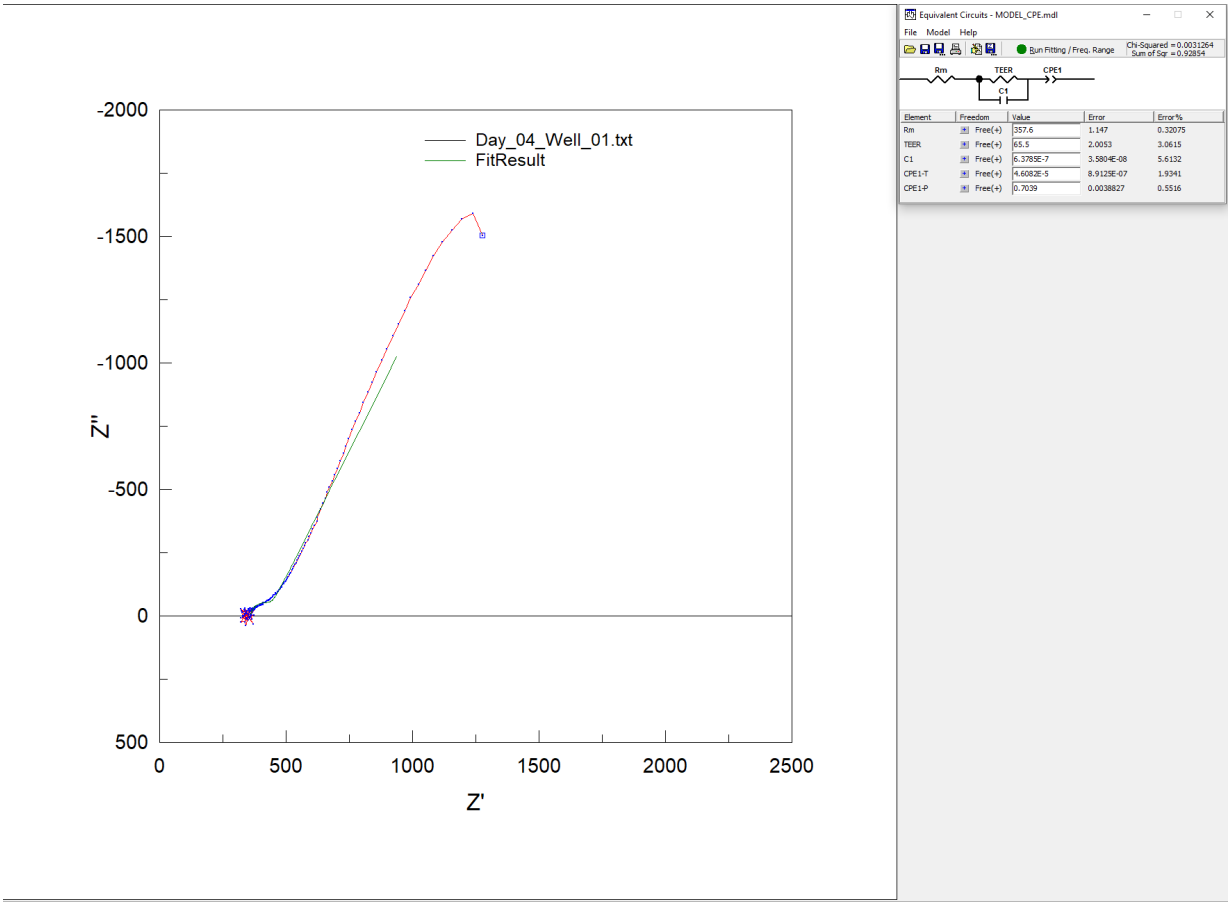

Fit Example using ZView.

Appendix D: Error Comparison

	TEER (Ohms)	Fit error	Average TEER (Ohms)	Standard deviation	Fit Error Average	Capacitance (F)	Fit error	Average Capacitance (F)	Standard deviation	Fit Error Average
Day 02 - Differentiated	59.27	0.80	61.74	2.10	0.89	8.62E-07	4.43E-09	7.13E-07	6.76E-08	3.89E-09
	61.58	0.89				6.99E-07	3.79E-09			
	65.52	1.01				6.79E-07	3.67E-09			
	61.58	0.94				6.80E-07	3.89E-09			
	59.62	0.97				7.24E-07	4.27E-09			
	62.36	0.94				7.62E-07	4.19E-09			
	61.58	0.81				6.43E-07	3.46E-09			
	64.28	0.90				6.46E-07	3.45E-09			
	59.9	0.78				7.21E-07	3.87E-09			

Error Comparison between triplicate measurements and fitting.